

INCREASING WATERFLOOD RESERVES IN THE
WILMINGTON OIL FIELD THROUGH IMPROVED
RESERVOIR CHARACTERIZATION AND RESERVOIR
MANAGEMENT

Annual Report 1996

By
Dennis Sullivan
Don Clarke
Scott Walker
Chris Phillips
John Nguyen
Dan Moos
Kwasi Tagbor

August 1997

Performed Under Contract No. DE-FC22-95BC14934

City of Long Beach
Long Beach, California



National Petroleum Technology Office
U. S. DEPARTMENT OF ENERGY
Tulsa, Oklahoma

DISCLAIMER

This report was prepared as an account of work sponsored by an agency of the United States Government. Neither the United States Government nor any agency thereof, nor any of their employees, makes any warranty, expressed or implied, or assumes any legal liability or responsibility for the accuracy, completeness, or usefulness of any information, apparatus, product, or process disclosed, or represents that its use would not infringe privately owned rights. Reference herein to any specific commercial product, process, or service by trade name, trademark, manufacturer, or otherwise does not necessarily constitute or imply its endorsement, recommendation, or favoring by the United States Government or any agency thereof. The views and opinions of authors expressed herein do not necessarily state or reflect those of the United States Government.

This report has been reproduced directly from the best available copy.

Available to DOE and DOE contractors from the Office of Scientific and Technical Information, P.O. Box 62, Oak Ridge, TN 37831; prices available from (615) 576-8401.

Available to the public from the National Technical Information Service, U.S. Department of Commerce, 5285 Port Royal Rd., Springfield VA 22161

DOE/BC/14934-7
Distribution Category UC-122

Increasing Waterflood Reserves In The Wilmington Oil Field Through Improved
Reservoir Characterization And Reservoir Management

Annual Report
March 21, 1995 to March 20, 1996

By
Dennis Sullivan
Don Clarke
Scott Walker
Chris Phillips
John Nguyen
Dan Moos
Kwasi Tagbor

August 1997

Work Performed Under Contract No. DE-FC22-95BC14934

Prepared for
BDM-Oklahoma/
U.S. Department of Energy
Assistant Secretary for Fossil Energy

Chandra Nautiyal, Project Manager
National Petroleum Technology Office
P.O. Box 3628
Tulsa, OK 74101

Prepared by:
City of Long Beach
Long Beach, California

Table of Contents

| <u>Description</u> | <u>Page</u> |
|------------------------|--|
| Forward | 1 |
| Abstract | 1 |
| Executive Summary | 1 |
| Introduction | 2 |
| Discussion | 2 |
| References | 11 |
| APPENDICES and FIGURES | 12 |
| APPENDIX 1 | Article placed in the AAPG guidebook for the national meeting |
| APPENDIX 2 | Paper titled "Viscoelasticity and Dispersion in Unconsolidated Reservoir Rocks from the Wilmington Field, California" |
| APPENDIX 3 | Paper titled "A Comparison of Dynamic and Static Moduli in Unconsolidated Reservoir Rocks from the Wilmington Field, California" |
| APPENDIX 4 | Paper titled "Hydrocarbon Saturation Determination from Sonic Log Data" |
| APPENDIX 5 | Paper titled "Identifying Patchy Saturation from Well Logs" |

Foreword

This project is intended to increase recoverable waterflood reserves in slope and basin reservoirs through improved reservoir characterization and reservoir management. The particular application of this project is in portions of Fault Blocks IV and V of the Wilmington Oil Field, in Long Beach, California, but the approach is widely applicable in slope and basin reservoirs. Transferring technology so that it can be applied in other sections of the Wilmington Field and by operators in other slope and basin reservoirs is a primary component of the project.

Abstract

This project uses advanced reservoir characterization tools, including the pulsed acoustic cased-hole logging tool, geologic three-dimensional (3-D) modeling software, and commercially available reservoir management software to identify sands with remaining high oil saturation following waterflood. Production from the identified high oil saturation sands will be stimulated by recompleting existing production and injection wells in these sands using conventional means as well as short radius and ultra-short radius laterals.

Although these reservoirs have been waterflooded over 40 years, researchers have found areas of remaining oil saturation. Areas such as the top sand in the Upper Terminal Zone Fault Block V, the western fault slivers of Upper Terminal Zone Fault Block V, the bottom sands of the Tar Zone Fault Block V, and the eastern edge of Fault Block IV in both the Upper Terminal and Lower Terminal Zones all show significant remaining oil saturation. Each area of interest was uncovered emphasizing a different type of reservoir characterization technique or practice. This was not the original strategy but was necessitated by the different levels of progress in each of the project activities.

Executive Summary

Waterflood oil recovery in the Wilmington Field has historically been inefficient due to a variety of factors, including reservoir heterogeneity, poor sweep efficiency, high water cut, and poor injection profiles. Sands with high remaining oil saturation are still present despite extensive waterflooding, but locating these sands has been difficult.

Reservoir management software has identified areas of potentially high remaining oil saturation in both the Upper Terminal Zone and the Lower Terminal Zone of Fault Block IV. A pulsed acoustic cased-hole logging tool was run in potential recompletion

candidates and recovered compressional wave data from which porosities were calculated. Unfortunately, shear wave data were not recovered therefore acoustically derived saturations cannot be predicted for the Fault Block IV wells. A standard remedial recompletion will be completed in each zone to validate the conclusions reached utilizing the reservoir management software.

Examination of recent electric logs (E-logs) revealed sands with remaining high oil saturation in the Tar Zone and Upper Terminal Zone of Fault Block V. A deterministic 3-D model was built around the Upper Terminal Zone recompletion candidate Well J-120. Well J-120 was recompleted and is undergoing steam consolidation as of this report date. A deterministic 3-D model was also built around the Tar Zone recompletion candidate Well J-15. Well J-15 was also recompleted and is undergoing steam consolidation as of this report date.

Initial results from the first four recompletions will be available for the next quarterly report.

Introduction

This project uses advanced reservoir characterization tools, including the pulsed acoustic cased-hole logging tool, geologic (3-D) modeling software, and commercially available reservoir management software to identify sands with remaining high oil saturation following waterflood. Production from the identified high oil saturation sands will be stimulated by recompleting existing production and injection wells in these sands using conventional means as well as short radius and ultra-short radius laterals.

Discussion

● Reservoir Characterization

Theoretical relationships, confirmed by laboratory and field data, suggest that hydrocarbon-bearing rocks in situ can be differentiated from rocks containing brines using sonic velocity measurements. Rock-log and fluid-log models are needed to calibrate, interpret, and understand the acoustic log data¹.

Because hydrocarbons in situ generally have much lower bulk moduli and densities than brines, replacing water with hydrocarbons lowers the compressional velocity and

increases slightly the shear wave velocity. Williams² presented convincing evidence that hydrocarbons could be detected from the difference between measured V_p/V_s and that predicted for a water saturated rock from shear wave velocity. Because the water delineation line is similar for clean and clay-bearing sands, virtually the same relationship can be used to detect hydrocarbons in both, eliminating the need for an independent lithology indicator. However, because of the lack of quantitative physical models to predict the effect, this technique has been applied with caution and a limited degree of success.

Researchers have developed a rock model which relates frame moduli to porosity in unconsolidated sands found in the Wilmington Field and other slope and basin reservoirs. However, this developed model assumes a uniform saturation in the pore space. Research is continuing to determine the effect on acoustic properties.

Monopole and dipole shear sonic logs can provide accurate compressional and shear wave velocities in cased holes, even in shallow, unconsolidated sands such as in the Wilmington Field. Porosity can be determined from shear wave velocity, provided an appropriate transform is used. Qualitatively, acoustic logs can be used to locate bypassed oil.

In practice, researchers have only been able to detect the shear wave in wells 167-W and M-499 out of six wells logged. Tube wave interference remains a formidable obstacle to overcome. An attempt to filter the wave with an absorber showed promise in a test well but failed in actual Wilmington well trials. The acoustic logging tool is being modified to overcome the tube wave interference.

● Reservoir Engineering

Injection and production data are still being input into the computer and quality controlled. This is an enormous task that we did not initially recognize. The input strategy has been altered and researchers are now concentrating on completing individual zones rather than the entire fault block at once.

The first zone completed was the Upper Terminal Zone of Fault Block IV. Injection and production data have been input, quality controlled, transformed into a database, and exported to Production Analyst reservoir management computer software. Researchers generated cumulative production bubble maps, cumulative injection bubble maps, daily production maps, and isocut maps. These maps revealed

an area on the east side of the fault block that appeared to have low cumulative oil recovery against the Harbor Entrance Fault. Idle well Y-63 penetrates the low recovery area and will be selectively recompleted in the Upper Terminal Zone across from the "Hx", "J", "Y", and "K" sands.

In zones where data input is not completed, researchers scanned the log files for newer electric logs which would indicate bypassed oil. Another technique employed to find bypassed oil was to identify anomalous production well characteristics such as lower than average water cuts, high oil production rates, and high water production rates. These techniques generated the X-32, J-15, and J-120 recompletion proposals.

Idle Well X-32 penetrates the Lower Terminal Zone of Fault Block IV and will be selectively recompleted across from the "AB", "AC", and "AD" sands. This prospect was generated from a well which was redrilled to a deeper production horizon and showed significant resistivities across the "AB", "AC", and "AD" sands. Surrounding Lower Terminal production wells produce with higher than field average oil cuts with good productivity. Also, X-32 penetrates the zone close to the Harbor Entrance Fault and could produce any oil that might be banked under and against the fault.

Fault Block V recompletion prospect J-15 was also generated from recent electric logs that passed through the Tar Zone and anomalous neighboring Tar Zone production wells. The "F₁" & "F_o" sands in this area of the Tar Zone in Fault Block V have not been completely drained. Electric logs from wells Z1-24, J-66, FJ-73, and J-46 show the resistivities have changed very little in the "F₁" sand and only moderately in the "F_o" sand from the 1960's until 1983. These wells reflect the saturations across a 1100 ft linear interval crossing just north of J-15. The 1982 E-log from nearby Well J-66, located 160 ft away, showed remaining oil saturation resistivities of 7 ohms in the "F₁" & "F_o" sands. The original J-15 resistivities of these same sands were 6 ohms in the "F₁" sand and 27 ohms in the "F_o" sand back in 1947.

Currently, there are two wells near J-15 that are selectively completed in the "F₁" & "F_o" sands, Z1-7 and J-7. Well Z1-7 is located 680 ft north of J-15 while J-7 is located 600 ft south of J-7. Z1-7 produces 76 b/d gross and 13 b/d net for an 82.9% water cut with 16 ft of fluid over the pump (FOP). J-7 produces 422 b/d gross and 11 b/d net for a 97.4% water cut with 1080 ft of FOP. J-7 hasn't produced up to expectations most likely due to the high FOP and resultant low pressure drawdown on the reservoir.

The proposed work for J-15 included extreme overbalanced perforating the 8-5/8" casing from 2310 ft ("F₁" + 8 ft) to 2345 ft ("F₂" + 25 ft) and consolidating the reservoir sand with one cycle of steam injection. Overbalanced perforating has been developed by Oryx Energy Company as a method to reduce skin damage. Sand consolidation with steam has been developed by Union Pacific Resources in the Wilmington Field. As of this report date, J-15 is undergoing the cyclic steam consolidation.

Fault Block V recompletion prospect J-120 was generated from recent electric logs that passed through the Upper Terminal. The "Hx₁" sand in this area of the Upper Terminal Zone has not been adequately drained. Electric logs from recently redrilled wells J-120, J-17, and J-46 show the resistivity has changed little from the 1960's until 1983. A 1983 E-log from J-120 showed remaining oil saturation resistivity at 7-8 ohms versus 12 ohms in 1961. The resistivity of the "Hx₁" sand in nearby Well J-17 has remained virtually the same at 9 ohms from 1964 until 1983. Only a few wells in the Upper Terminal Zone have been open to production in the subject sand. Currently, Well A-52 is the only well able to produce from this sand. A-52 is almost 1000 ft away from J-120 and located on the other side of the structure. Also, there has been little or no water injection into this sand east of the Maine Avenue Fault. On the east side of the Maine Avenue Fault, the "Hx₁" varies from 20 ft to 30 ft in gross thickness and is well developed with good remaining oil saturation. Areally, this covers about one half of the Upper Terminal Zone in Fault Block V. The "Hx₁" sand is wet and not as well developed on the west side of the Maine Avenue Fault. The original "Hx₁" oil-water contact is located far to the south of J-120.

The proposed work for J-120 included extreme overbalanced perforating the 7" casing from 2993 ft ("Hx₁" - 3 ft) to 3009 ft ("Hx₁" + 19 ft) and consolidating the sand with one cycle of steam injection. As of this report date, J-120 is undergoing the cyclic steam consolidation.

● Deterministic 3-D Geologic Modeling

Researchers also changed strategy on the geologic 3-D modeling to focus on specific areas within a zone and fault block for directional survey data input, fault picks, and sand marker picks. Midway through the data input a serious problem was uncovered with the NEWILMA program code and database used to build the deterministic geologic 3-D model. The problem involved the subsidence correction when NEWILMA calculates the vertical subsea depth (VSS) from the well directional survey. Depths are supposed to be increased by adding the subsidence components.

There are three parts to the subsidence correction. The first part is a correction to the surface site to the elevation of the ground level when the well was drilled. The second part is to correct the marker (based on the X, Y location) by adding the subsidence that occurred between the time the well was drilled and the present. The third part subtracts the compression due to fluid withdrawal from the oil sands. The original subsidence correction subroutine had calculated an incorrect value for the subsidence from when the well was drilled to the present, did not correct for the surface change between 1937 and when the well was drilled, and did not address the compression of the sands. The subsidence subroutine was successfully altered and the program recompiled.

Earth Vision software has generated structural contour maps of the Upper Terminal Zone in Fault Block V at the "Hx₁, Hx₀, Hx₂, and Hx" sand markers. All penetrating wells had their electric log examined and had these sands markers identified and entered into the Earth Vision NEWILMA database. Researchers are now working on isopach maps for these same horizons as part of the deterministic geologic model. The first version of the deterministic geologic model for the J-120 recompletion prospect is shown in Figure 1.

A deterministic geologic model has also been generated for the Upper Terminal Zone Fault Block IV prospect at the "Hx" sand marker (Fig. 2). It shows recompletion candidate Y-63 penetrates the Upper Terminal Zone just to the west of the Harbor Entrance Fault. Researchers theorize oil is banked up against the Harbor Entrance Fault and can be captured by Y-63.

● Pulsed Acoustic Logging

Well M-499 was drilled in 1993 as an infill well to produce the Upper Terminal Zone of Fault Block IV. It was logged both open hole and cased hole with a comprehensive log suite³. Excellent open hole sonic data were obtained. Cased hole compressional and shear logs from the MPI (XACT) tool were similar to open hole results. Cased-hole shear data required filtering to remove a strong tube wave arrival prior to processing the data. The XACT tool used in this well had an early version of the receivers without calibration and acceleration correction, and with downhole (analog-domain) summing/differencing to enhance monopole or dipole energy, respectively. The XACT source was an old version with a center frequency in P of about 3 kHz and in S of 1.2 kHz.

The casing bond tool (CBT) revealed excellent bond in the zone of interest. There

was little casing arrival, and a well developed formation arrival could be seen throughout much of the hole. The Ultra-Sonic Imager (USI) showed moderately good cement bond but some fluid behind the casing.

Recompletion candidate well FY-67 was logged with the MPI tool and the Schlumberger tool. A dogleg in the well at 1560 ft made passage of the MPI tool difficult, and the centralizers on the tool were removed and replaced with wraps of duct tape. Compressional waveforms recorded by the Dipole Shear Imager (DSI) and the XACT agree quite well except where low amplitudes confuse the analysis. DSI Lower Dipole data are better than Upper Dipole data, but no reliable shear velocities could be determined in either case. The XACT tool did not provide shear velocities either.

The USI tool revealed fairly poor bonds, lots of water behind casing, above 3000 ft. Below the 3000 ft mark average bond appears to be better than in well M-499 with relatively few intervals in which fluid is predicted behind casing. There was a distinct difference in bond quality between the upper and lower sides of the hole, with the low side having better bond. Throughout the well there were indications of gas behind casing, but in amounts less than indicated in well M-499.

Inspection of the Schlumberger monopole data reveals a significant early casing arrival throughout much of the hole, although a good formation arrival can be seen later in the wave train. The change at 3000 ft is also clear on the waveforms; below that depth the casing arrival is less distinct. If this can be compared directly to the CBT results in well M-499, it suggests a much worse bond in well FY-67, in contrast to the USI data which indicated a slightly better bond.

An attempt to re-log the well with a modified MPI XACT tool was terminated when the tool could not pass through the known dogleg at 1560 ft.

Well 167-W was originally drilled in 1983 with a deviation of 28-32 degrees. Steel casing extends down to 4032 ft, below which a slotted fiberglass liner was installed for sand control and corrosion protection. It was logged twice with the MPI XACT tool and once with the Schlumberger DSI tool along with a USI for cement bond evaluation. Compressional waveforms recorded by the DSI and XACT show similar variations downhole. Velocities determined from the monopole data of both tools agree quite well except where low amplitudes confuse the analysis. DSI Lower Dipole data are better than Upper Dipole, but no reliable shear velocities could be determined in either case. The XACT data did not provide shear velocities either. DSI data provided compressional and probable shear velocities in the fiberglass section

of the hole.

The USI reveals quite variable casing bond in well 167-W. Bond is similar to that of well M-499. Unlike well FY-67, there is no clear difference in bond quality between the upper and lower sides of the wellbore.

Recompletion candidate well X-32 was logged with the MPI XACT tool. This well was originally drilled in 1946. No shear wave data were obtained, but reasonable compressional wave velocities were determined from the monopole data.

Recompletion candidate well Y-63 was logged on two separate occasions with the XACT tool. Neither compressional nor shear wave velocities could be determined from the first logging sequence. A return visit with a modified XACT tool and tube wave absorber also did not yield acceptable data. Fourteen different combinations of receivers, sources, spacers, and attenuators were tried and did not reproduce the data from the first logging sequence.

The XACT tool has been undergoing a number of design modifications since the initial logs were recorded in well M-499 in 1993. The original tool had four "receivers", each of which consisted of 4 crystals mounted at 90° intervals. To record monopole data the signals from crystals mounted 180° apart in line with the source are summed downhole. To record dipole data the crystals from receivers mounted 180° apart in-line with the source are differenced downhole. The receivers are not calibrated, so the sums and differences do not perfectly discriminate the appropriate phases. The source is a pulse of fluid which acts across a membrane on the wellbore fluid, in such a way that it is in phase across the tool in monopole mode and out of phase across the tool in dipole mode. The source was not perfectly "balanced", so some monopole energy is generated in dipole mode, and some dipole energy is generated in monopole mode. In compressional mode the center frequency is about 3 kHz. In dipole mode the center frequency is about 1.2 kHz.

A number of design changes were made to the XACT tool prior to logging the first wells in this project. First a new receiver section was developed, in which the crystals were remounted to cancel accelerations imparted to the body of the tool by the fluid in the borehole. Also, the receivers were calibrated to improve the summing and differencing to enhance mode discrimination. Finally, the receivers were configured so that summing or differencing could be achieved uphole (A and C mode) or downhole (A + C mode; A-C mode). A new source (XMTR) was developed which was more carefully balanced to produce pure monopole or pure dipole energy. This

source also generated significantly more energy in each pulse. And, it was modified to generate a dipole mode with a center frequency of about 800 Hz. This tool was run during August 1995 in holes OB2-3, 167-W, FY-67, X-32 and Y-63. In several of these holes the original transmitter was also run for comparison.

In general, data from the original transmitter appears to be better because it excites less low frequency (~ 600 Hz) tube wave energy.

A tube-wave absorber was developed to attenuate fluid-borne energy. This section was re-run in FY-67 (it didn't get past the dogleg) and Y-63 in December 1995. Based on data recorded at 350 ft in a test well at Stanford, the maximum amplitude reduction using one absorber is about 3x (10dB), with little attenuation outside the stop band (250-1750 Hz).

Schlumberger's DSI tool records on 8 receivers up- and down-going dipole data from two different sources, mounted 90° to each other, and monopole (higher-frequency) data from a third source. All three data sets are analyzed independently using STC processing. Log quality control consists of color displays of the coherence as a function of slowness with picks, and the filtered waveforms as a function of time.

Receiver data are differenced or summed downhole, thereby making it difficult to unambiguously determine the mode type where dipole and tube/Stonely waves interfere.

● Technology Transfer

Technical transfer activities included a field trip to the Wilmington Field for the American Association of Petroleum Geologists (AAPG) in association with their 1996 national meeting in San Diego. An article was also placed in the AAPG guidebook for the national meeting (APPENDIX 1).

Researchers are also planning the Stanford Rock and Borehole Geophysics Project Annual Meeting. Papers written and presented will include:

"Viscoelasticity and Dispersion in Unconsolidated Reservoir Rocks from the Wilmington Field, California" (APPENDIX 2)

"A Comparison of Dynamic and Static Moduli in Unconsolidated Reservoir Rocks from the Wilmington Field, California" (APPENDIX 3)

"Hydrocarbon Saturation Determination from Sonic Log Data" (APPENDIX 4)

"Identifying Patchy Saturation from Well Logs" (APPENDIX 5)

Tidelands Oil and USC are developing a CD-ROM multimedia presentation on the history of this project. This historical record will be updated continuously and available to other operators and the public in general. Periodically, CD's would be produced and distributed to other organizations as part of our technical transfer commitment. In addition, Stanford has placed a "home page" of the SPE paper and the DOE project on the World Wide Web.

Chris Phillips, Chief Geologist with Tidelands, made a presentation on the 3-D deterministic geologic model entitled "Application of Advanced Reservoir Characterization to Increase the Efficiency of a Thermal Steam Drive in the Wilmington Oil Field, California" at the 1995 AAPG Pacific Section Meeting in San Francisco, CA. on May 3-5, 1995. Don Clarke and Mike Henry of the City of Long Beach were co-authors.

Dan Moos of Stanford was in New Orleans on May 18, 1995 speaking at the Society of Professional Well Log Analysts (SPWLA).

Several articles were published in trade journals and newspapers about this DOE project. Articles were published in the October 10, 1994 edition of the Long Beach Press - Telegram newspaper, in the October, 1994 issue of the SPE Los Angeles Basin Section Newsletter, in the December, 1994 issue of World Oil magazine, and in the March, 1995 issue of Petroleum Engineer International magazine.

Tidelands, the City of Long Beach, and USC held a technical transfer meeting of DOE Class III participants on May 15, 1995 in Valencia, CA to discuss their desire to have specific joint activities, such as the 1996 AAPG National Meeting, the 1997 SPE Western Regional Meeting, and the 1998 Joint SPE Western Regional/AAPG Pacific Basin Section Meeting. Tidelands and City of Long Beach personnel have already begun work on these meetings to promote technical sessions on slope and basin clastic reservoirs, advanced reservoir characterization, and enhanced oil recovery.

Scott Hara of Tidelands sent out a letter to California Coastal members of AAPG on January 10, 1995 announcing our DOE projects and to contact him to be placed on a mailing list of future technical transfer activities.

References

1. D. Moos, J. Dvorkin, A. Hooks, *Application of Theoretically Derived Rock Physics Relationships for Clastic Rocks to Log Data - Example from the Wilmington Field, CA*, paper prepared for special issue of Geophysical Research Letters on Core/Log/Seismic Integration, January 1996.
2. D. Williams, *The Acoustic Log Hydrocarbon Indicator*, paper W for Society of Professional Well Log Analysts 31st Annual Logging Symposium, June 1990.
3. D. Moos, S. Hara, C. Phillips, A. Hooks, K. Tagbor, *Field Test of Acoustic Logs for Measuring Porosity and Oil Saturation in a Mature Waterflood in the Wilmington Field, CA*, paper SPE 29655 presented at the Society of Petroleum Engineers Western Regional Meeting, Bakersfield, CA, March 1995.

DETERMINISTIC MODEL FAULT BLOCKS 5 AND 6

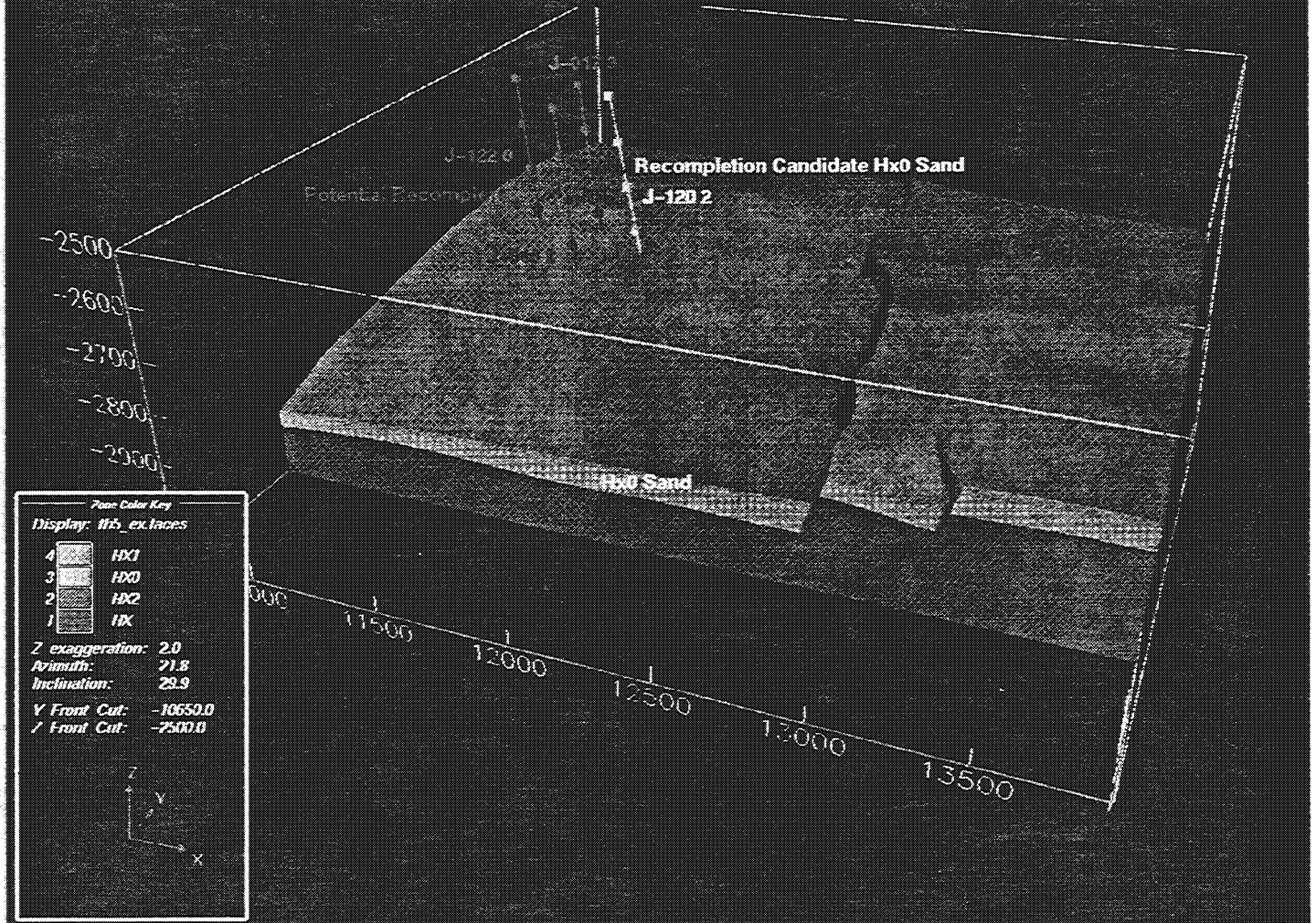


FIGURE 1

DETERMINISTIC MODEL

FAULT BLOCK 4

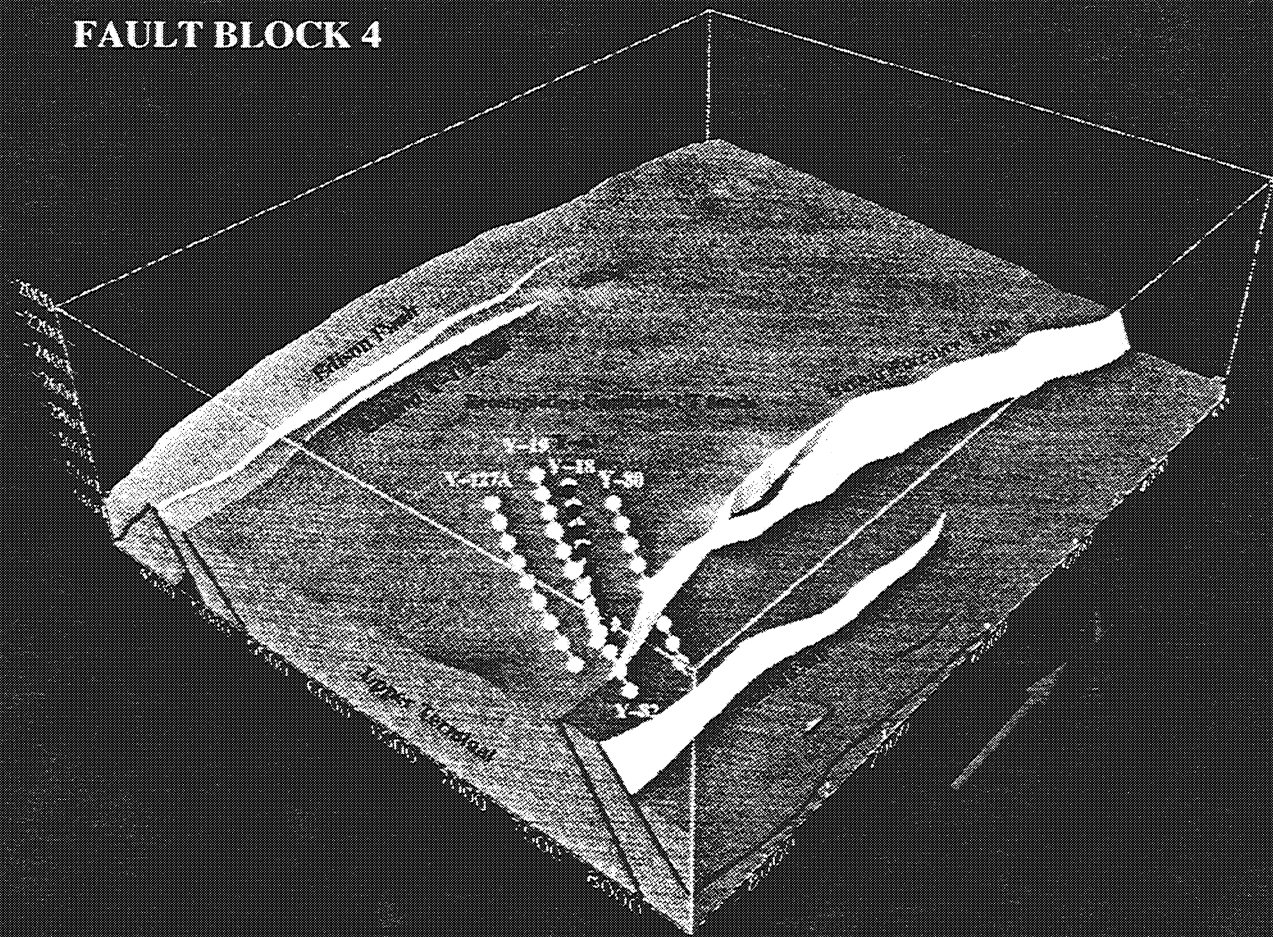


FIGURE 2

Sonic Logging to Detect Bypassed Hydrocarbons in the Wilmington Field, CA

Daniel Moos
Stanford University
Department of Geophysics
Stanford, CA 94305-2215

F. Scott Walker
Tidelands Oil Production Company
Long Beach, California

Donald D. Clarke
Department of Oil Properties
Long Beach, California

INTRODUCTION

Theoretical relationships, confirmed by laboratory and field data, suggest that hydrocarbon-bearing rocks in situ can be differentiated from rocks containing brines using sonic velocity measurements. A project to test this technique has been undertaken in the Wilmington Field, California, with co-funding from the Department of Energy (DOE cooperative agreement no. DE-FC22-95BC14934). Models, using values of fluid and formation properties typical of the Miocene-age turbidites within the target interval, confirmed that it should be possible to differentiate between hydrocarbon and non-hydrocarbon bearing sands in this field using compressional and shear wave sonic velocity logs. To date six wells (ranging in age up to 50 years) have been logged through casing with a multipole sonic logging sonde. Velocities measured in the open hole agreed with those measured after casing was installed in the most recently drilled well. Although compressional velocities have been determined in all but one case, shear-wave velocities have been obtained in only two of the six wells. Predictions of oil saturation are in qualitative agreement with models and prior measurements. However, one surprising result is that porosity can be determined from shear-wave velocity logs through casing. This may prove to be important in the future when through-casing resistivity logs become commercially available.

The Wilmington Field

The Wilmington field is located within a NW-SE trending faulted anticline beneath and immediately

offshore of Long Beach, CA (Figure 1). The first successful well was drilled in 1932. As of 1994, more than 2.5 billion bbls of oil and 1.2 billion Mcf of gas had been produced, and it was believed that more than 1.8 billion bbls of oil still remained. Initial production was enhanced by a waterflood started in the 1950's primarily to mitigate surface subsidence which had reached more than 29 feet in the center of the bowl directly overlying the region of greatest production (Colazas and Strehle, 1995). Injection wells and production wells are located throughout the field, and production primarily continues from the center.

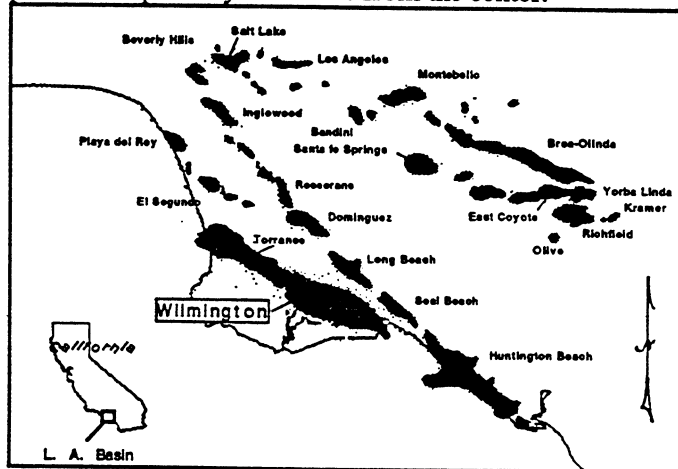


Figure 1: Location map, showing the Wilmington Field and other oil fields within the Los Angeles Basin (after Mayuga, 1968).

Production at Wilmington is from a thick sequence of clastic basin and slope sediments (unconsolidated, low maturity, turbiditic arenites and clean arenites with porosities exceeding 25% and permeabilities of 100's to 1000's of millidarcys, interlayered with sandy clays (wackes) containing 50%

or more detrital smectite (Henderson, 1987 and Norton and Otott, 1996)). The producing horizons lie between depths of 2250 and about 10000 feet. The hydrocarbons produced at Wilmington range from 12° API gravity (Tar zone) to 18°-19° API gravity (Ranger and Upper Terminal Zones) to 27° API gravity (Lower Terminal). API gravities as high as 30 are produced from deeper sections of the field (the Union Pacific, Ford, and 237 zones).

Theoretical Basis of the Sonic Detection Technique

Generally, when a rock is loaded under an increment of compression, such as from a passing seismic wave, an increment of pore pressure change is induced, which resists the compression and therefore stiffens the rock. The low-frequency Gassmann (1951) - Biot (1956) theory predicts the resulting increase in effective bulk modulus, K_{sat} , of the saturated rock:

$$\frac{K_{sat}}{K_0 - K_{sat}} = \frac{K_{dry}}{K_0 - K_{dry}} + \frac{K_f}{\phi(K_0 - K_f)} \quad (1)$$

where ϕ is the porosity and K_0 , K_f , and K_{dry} are the bulk moduli of the mineral material, the pore fluid, and the dry rock, respectively. Gassmann predicted no change for the isotropic shear modulus with saturation, $\mu_{sat} = \mu_{dry}$. The bulk and shear moduli are related to the compressional wave velocity, V_p , shear wave velocity, V_s , and density, ρ , through the familiar equations:

$$V_p = \sqrt{\frac{K + \frac{4}{3}\mu}{\rho}} \quad V_s = \sqrt{\frac{\mu}{\rho}} \quad (2)$$

Equation (1) assumes a homogeneous mineral modulus and statistical isotropy of the pore space, but is free of assumptions about the pore geometry. Most importantly, it is valid only at sufficiently low frequencies such that the induced pore pressures are equilibrated throughout the pore space (i.e., that there is sufficient time for the pore fluid to flow and eliminate wave-induced pore pressure gradients).

These theoretical predictions have been confirmed qualitatively by a number of field studies. For example, seismic detection of free gas exploits this fluid effect because the abrupt increase in fluid compliance due to the gas generates a very large P-wave impedance contrast, producing a "bright spot" on a reflection seismic record. More recently, bright spots have also been observed to occur at oil/water interfaces (Clark, 1990). Using sonic P- and S-wave velocity logs, Williams (1990) demonstrated an Acoustic Log Hydrocarbon Indicator (ALHI) which was based on the difference between measured V_p/V_s and that predicted for a water-saturated rock from the shear-wave velocity. More recent results indicate that elastic properties may vary systematically with saturation (Hornby and others, 1992).

Predictions for Wilmington

The ability to detect hydrocarbons using elastic waves depends both on the amount by which their properties differ from those of brines and the degree to which those properties control the velocities of the saturated rock. Several factors influence the properties of the fluids at reservoir conditions. In general, density, bulk modulus and viscosity all decrease with increasing API number (decreasing density) and temperature and increase slightly with increasing pressure. Gas in solution has a large effect, even in comparison to that of temperature, in reducing density and bulk modulus. Using equations presented in Batzle and Wang (1992), it is straightforward to determine the properties of reservoir fluids.

These can then be applied, using the Biot-Gassmann relations, to predict the elastic-wave velocities as a function of depth. Figure 2 shows the predicted shear and compressional velocities and the velocity ratios as a function of depth and pore fluid for an assumed porosity of 30%. These results suggest that, for basin clastics such as those found at Wilmington, seismic velocities are quite sensitive to the properties of the pore fluids. And, for the expected properties of the actual pore fluids, the sonic detection technique should be quite successful at differentiating between sands with high saturations and those in which the hydrocarbons have largely been replaced with water.

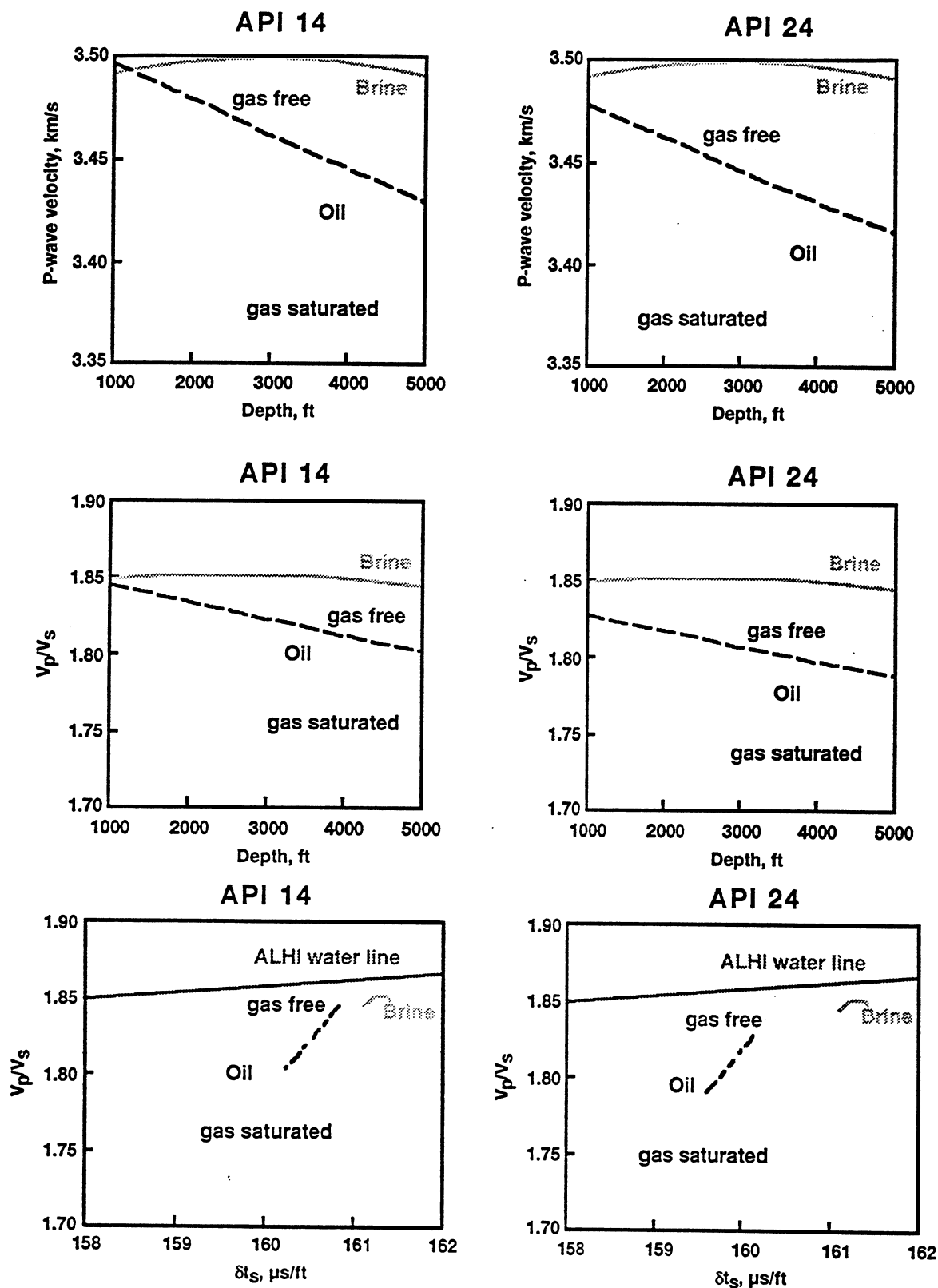


Figure 2: Elastic-wave velocities predicted for a 30% porosity Wilmington sand saturated with various pore fluids (after Moos, and others, 1995). Also shown are cross plots of V_p/V_s vs. δt_s , including the Williams (1990) ALHI water line for comparison.

Results in M-499

Well M-499 was completed in the Upper Terminal Zone of Fault Block IV in an area previously considered to be watered out. To evaluate the production potential from a selective recompletion of an existing well, M-499 was perforated only in sands with oil saturations above 40%, based on the analysis of open-hole well logs. New high power, low frequency (1.2-2.5 kHz) monopole and dipole sonic logs (Chen and Eriksen, 1991) were recorded to evaluate their ability to measure formation porosity and oil saturation through casing as a guide in carrying out selective recompletions in existing wells. Compressional-wave velocities were determined from analysis of monopole waveforms. Shear-wave velocities were determined through analysis of the dipole waveforms.

The very high energy and low center frequency of the source results in a depth of investigation which is more than ten times that of typical sonic logs (up to two meters), allowing data to be recorded in both open and cased holes. By exciting dipole modes in the wellbore, shear-wave velocities can be determined even in "slow" formations (that is, with shear-wave velocity below 1.5 km/s or shear-wave slowness (dt_s) above 200 μ s/ft). In addition, by separately recording the waves on opposite sides of the tool, one can differentiate between true dipole modes, which provide information on the shear-wave velocity, and tube waves, which can interfere with the dipole mode in cased holes.

Sonic data were recorded in M-499 both before and after the installation of casing (Moos, and others, 1995). The velocity data presented here were determined from the cased-hole measurements. A comprehensive suite of open-hole logs was also recorded in the well to guide in completion decisions and for comparison to analyses of porosity and saturation using the sonic data.

Porosity

It is generally accepted that in hard rocks conventional (compressional-wave) sonic logs can be used to determine porosity through the use of the Wyllie time-average equation or Raymer's relationship. However, experience has demonstrated that these techniques cannot be used to determine porosity in

fields such as Wilmington. This is largely because of the unconsolidated nature of the rocks in these fields (Moos, and others, in press). Furthermore, dt_p is affected both by porosity and by other factors such as fluid properties. Because the shear wave is (theoretically) relatively unaffected by the fluid, it should be possible to derive a porosity log from dt_s , provided an appropriate model is used to relate porosity to velocity.

A further benefit of using shear-wave velocity to determine porosity is that such logs can be run through casing. In most instances. Sonic logs have a much greater radius of investigation than nuclear logs (Westaway, et al., 1981), making the result from shear-wave analysis a more reliable predictor of formation properties away from the near-wellbore zone.

Figure 3 shows porosity derived from shear-wave velocity using techniques described in Moos and others (in press) for the entire logged interval in M-499. Also shown are porosities derived from empirical relationships (Moos, and others, 1995) and from the density log. There is excellent agreement throughout most of the logged interval between the different porosity measures, with the exception of washed-out sections within which the density log reads anomalously small values leading to overly large porosity estimates.

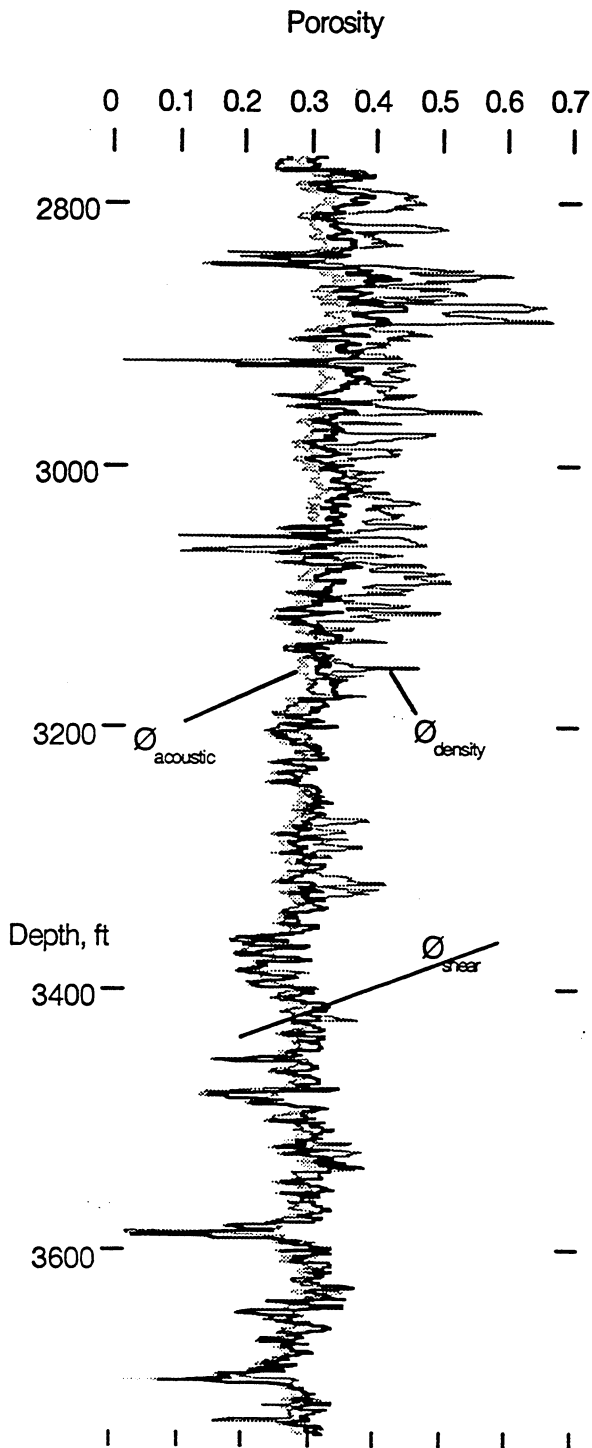


Figure 3: Porosity determined from a density log (ϕ_{density}), from an empirical relationship developed using other data (ϕ_{acoustic}) (Moos, and others, 1995), and from the theoretical relationship described in Moos et al. (in press); (ϕ_{shear}). In general, there is excellent agreement between the two sonic porosity measures, whereas the density porosity is generally slightly greater, likely due in shallow sections to poor pad contact in the rugose hole.

Saturation

Figure 4 compares the ALHI water lines of Williams (1990) to data from the Upper Terminal section of M-499. Based on Williams' analysis and Biot-Gassmann, oil-bearing units are predicted to lie below the water lines. As can be seen, a significant percentage of the depth interval logged is predicted to be oil-bearing.

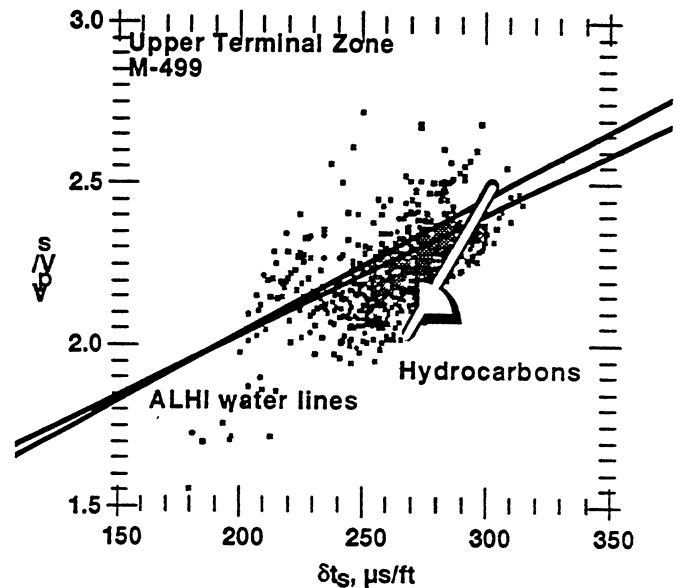


Figure 4. Crossplot of V_p/V_s vs. dt_s showing the ALHI water lines of Williams, compared to data from the Upper Terminal of well M-499.

In Figure 5 the normalized distance from the water line is compared to saturation determined using Archie's Law for the Upper Terminal Zone. There is qualitative agreement between the two curves, with the exception of some intervals which are predicted to have high oil saturations based on the sonic data, but which do not appear to have high oil saturation based on the conventional log analysis. These zones can largely be eliminated from consideration for recompletion using geological constraints, data from recent offset wells, and production experience. Of more importance is the observation that the intervals chosen for completion based on the conventional analysis are also predicted to have high oil saturation based on the sonic results.

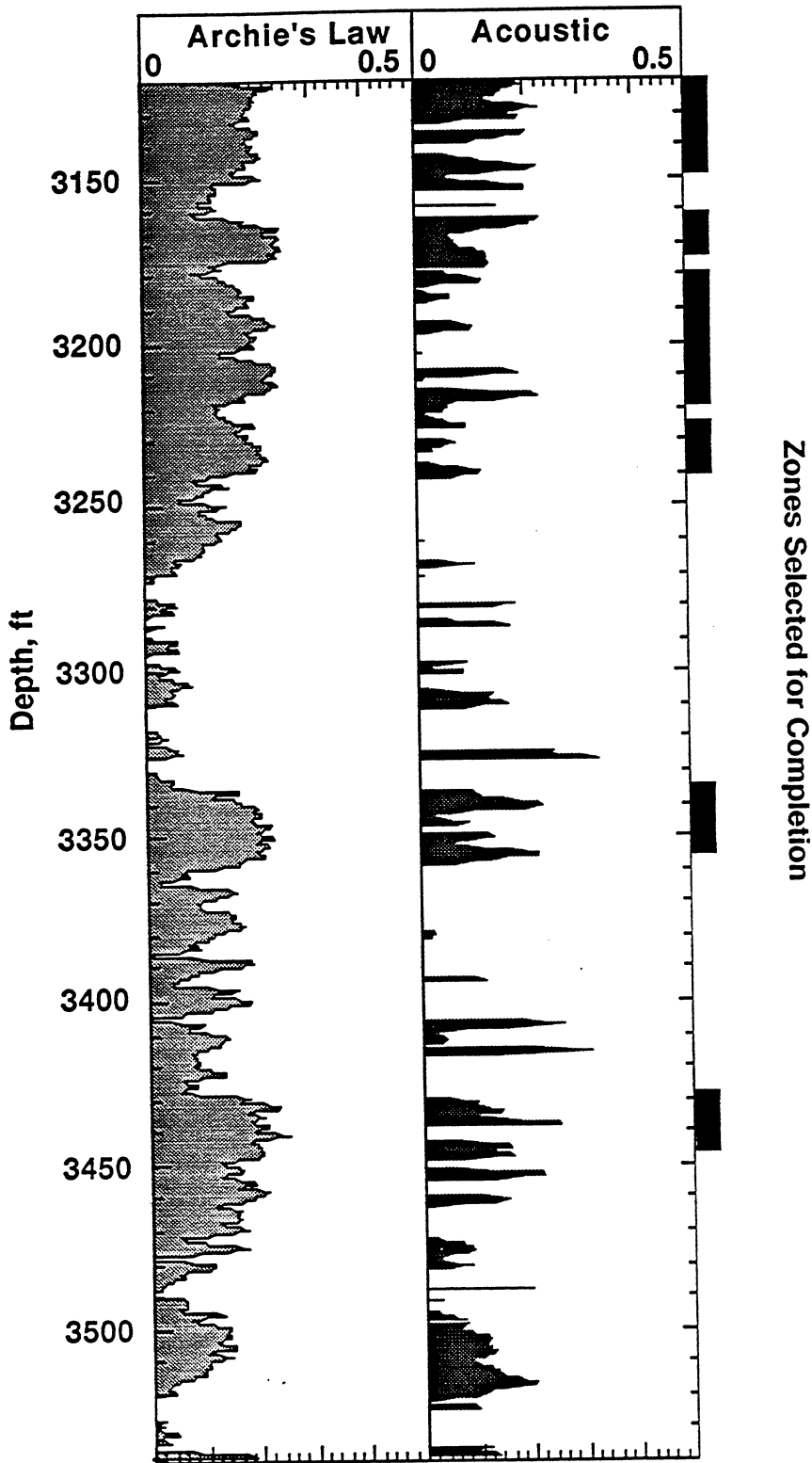


Figure 5. Saturation predictions based on Archie's Law and on the sonic data. Also shown are the intervals chosen for completion based on the Archie's Law analyses.

Results in Other Wells

Although the results from M-499 are promising, it is necessary to demonstrate first that it is possible to routinely obtain the sonic data necessary for this analysis, and second that the sonic technique can accurately differentiate between watered-out and potentially productive zones. To accomplish this the sonic logs were run in five more holes as summarized in Table I. Prior to running these additional logs the tool was modified to improve receiver characteristics and to allow independent recording of wave arrivals on opposite sides of the tool.

Table I: Summary of hole characteristics.

| Well | Depth Interval, kft | Deviation | Year Drilled | Well Type |
|-------|---------------------|-----------|--------------|-------------|
| M-499 | 2.8-3.7 | 43° | 1993 | Prospect |
| 167-W | 2.5-4.5 | 30° | 1983 | Water flood |
| FY-67 | 1.6-3.7 | 17° | 1948 | Water flood |
| Y-63 | 1.6-3.2 | 17° | 1948 | Prospect |
| X-32 | 3.0-5.6 | 17° | 1946 | Prospect |
| J-15 | 1.2-2.9 | vertical | 1942 | Prospect |

Compressional-wave velocities were determined in all of these wells except in Y-63. In contrast, shear-wave velocities could be determined only in M-499 and in the uppermost few hundred and lowermost several hundred feet of well 167-W. In the intermediate depth range within 167-W (from about 2900 to 3300 feet) the shear wave arrived at the same time and was characterized by the same frequency content as the interfering tube wave. In 167-W, the ability to record independently the wave arrivals on opposite sides of the tool was essential for differentiating between tube wave and the dipole mode.

Thus it appears that the critical determinants of the success of shear-wave logging are: (1) the age of the well, and (2) the shear-wave velocity. Deviation, leading to eccentricity of the tool in the casing, and the casing in the hole, does not appear to be a problem in spite of the inevitable additional generation of tube-wave energy by the dipole source. Further study is needed to determine if factors such as the casing diameter and the cement thickness and bonding to the formation affect the quality of the dipole data.

Neither standard casing bond logs nor specialty logs which measure the azimuthal variation of bond using acoustic techniques provided clear predictions of the quality of the sonic logs.

CONCLUSIONS

Based on the results so far, three conclusions can be reached. First, porosity can be determined accurately using shear-wave velocity in reservoirs such as Wilmington, provided the appropriate model for their relationship is used. Second, cased-hole shear-wave logging in formations such as the Wilmington sands is extremely difficult, due both to wellbore conditions and to the similarity of the dipole mode moveout and that of the tube wave. Furthermore, discrimination between these two modes, even where their moveout is different, requires separate recording of arrivals on opposite sides of the tool to verify wave mode symmetry. However, it is clear that if the data can be recorded it is possible to discriminate between watered out and potentially productive zones. Additional analysis of the data so far recorded and of new data will help to refine these preliminary conclusions.

REFERENCES CITED

- Batzle, M., and Wang, Z., 1992, Seismic properties of pore fluids: *Geophysics*, v. 57, p. 1396-1408.
- Biot, M.A., 1956, Theory of elastic waves in a fluid-saturated porous solid, II. Higher frequency range: *J. Acoust. Soc. Am.*, v. 28, p. 179-191.
- Chen, S.T., and Eriksen, E.A., 1991, Compressional and shear-wave logging in open and cased holes using a multipole tool: *Geophysics*, v. 56, p. 550-557.
- Clark, V.A., 1990, The effect of oil under in situ conditions on the seismic properties of rocks: *Geophysics*, v. 57, p. 894-901.
- Colazas, X. C., and Strehle, R. S., 1995, Subsidence in Wilmington Oil Field, Long Beach, California, USA, in Chilingarian, G. V., Donaldson, E. C., and Yen, T. T., eds., *Subsidence of Petroleum Reservoirs Due to Fluid Withdrawal*, Elsevier Science, Amsterdam, The Netherlands, p. 285-335.
- Gassmann, F., 1951, Über die elastizität poroser medien: *Vierteljahrsschr. Naturforsch. Ges. Zuerich*, v. 96, p. 1-23.

- Henderson, C. P., 1987, The Stratigraphy of the Wilmington Oil Field, *in* Clarke, D. D., and Henderson, C. P., eds., Oil Producing Areas in Long Beach: Pacific Section, American Association of Petroleum Geologists Geologic Field Guide to the Long Beach Area, p. 57-68
- Hornby, B.E., W. F. Murphy, I., Liu, H.-L., and Hsu, K., 1992, Reservoir sonics: A North Sea case study: Geophysics, v. 57, p. 146-160.
- Mayuga, M.N., 1968, Geology and Development of California's Giant - The Wilmington Oil Field, AAPG 53rd Ann. Meeting, Oklahoma City, OK, p. 47.
- Moos, D., Dvorkin, J., and Hooks, A., in press, Application of Theoretically Derived Rock Physics Relationships for Clastic Rocks to Log Data - Example from the Wilmington Field, CA: Geophys. Res. Lett.
- Moos, D., Hara, S., Phillips, C., Hooks, A., and Tagbor, K., 1995, Field test of acoustic logs for measuring porosity and oil saturation in a mature waterflood in the Wilmington Field, CA, SPE 29655, SPE Western Regional Meeting, Bakersfield, CA.
- Norton, T. A. and Ottot, G. E., 1996, The Stratigraphy of the Wilmington Oil Field, *in* Clarke, D. D., Ottot, G. E., and Phillips, C. C., Old Oil Fields and New Life: A Visit to the Giants of the Los Angeles Basin, Guidebook, Division of Environmental Geology, Pacific Section, American Association of Petroleum Geologists, and the Society of Petroleum Engineers, in press.
- Westaway, P., Wittmann, M., and Rochette, P., 1981, Application of nuclear techniques to reservoir monitoring: Journal of Petroleum Technology, Jan 1981, p. 46-54.
- Williams, D.M., 1990, The acoustic log hydrocarbon Indicator *in* SPWLA 31st Annual Logging Symposium, June 24-27, Paper W.

PAPER G7**VISCOELASTICITY AND DISPERSION IN UNCONSOLIDATED
RESERVOIR ROCKS FROM THE WILMINGTON FIELD, CALIFORNIA****Carl T. Chang****Mark D. Zoback****Dan Moos***Stanford Borehole Geophysics Laboratory***ABSTRACT**

Dry turbidite sand samples from the Wilmington field, Long Beach, California, exhibited creeping behavior in load controlled creep tests. Creep occurred at hydrostatic loads of 10 - 30 MPa, and axial loads of 4 MPa with 20 MPa confinement. Creeping time constants were approximately 10 hours. Ottawa sand samples tested in a similar manner do not exhibit creep. A standard linear solid model was fitted to the turbidite creep test data to determine if the difference between static and dynamic moduli measured in Paper G6 could be attributed to viscoelasticity, and to calculate the frequency dependent modulus. Based on the model, the crossover point from high to low frequency response came at .001 Hz, which reflects the high viscosity of these dry rocks. The close fit to the experimental data suggests that viscoelasticity may be responsible for the dispersion detected in the Wilmington Upper Terminal zone turbidite samples.

INTRODUCTION

Although viscoelasticity has been extensively documented in soil mechanics, the phenomenon has been traditionally associated with dewatering of saturated soils (Terzaghi, 1936). Terzaghi established that the reduction of void ratio in a saturated clay soil results in a transient pore pressure that carries the load. This pressure, known as the hydrostatic excess pressure, is dissipated at a rate which depends on the permeability of the soil mass and the load is eventually transferred to the soil structure in the consolidation process. Soil engineers use the oedometer consolidation test (El Refai, 1978) to study this time

dependent deformation. This simple test is a step load uniaxial strain (i.e., laterally constrained) test on a cylindrical sample in the drained state. This behavior is dependent on fluid saturation. Thus, it is unusual to observe time dependent consolidation oedometer tests on a dry and highly permeable sand. Dry sand creep is peculiar and unexpected in our pressure and temperature ranges since there is no hydrostatic excess pressure. Since creep is a manifestation of viscoelasticity, an alternate mechanism besides poroelasticity must be responsible for dry creep.

Viscoelasticity is clearly an important mechanism responsible for dispersion in saturated cemented rocks (Bourbie, 1987). Previous results investigating frequency dependent moduli in cemented rocks (Winkler, 1983) have established a relationship between the presence of pore fluids and matrix stiffness. The resulting dispersion is believed to be caused by inertial effects of the fluid moving in the pore volume (Biot, 1956, Mavko and Nur, 1979). Higher frequencies result in higher elastic stiffnesses. It is not obvious why a dry sample would display viscoelasticity, since it is generally understood to result from fluid saturation.

Dry rock creep is a crystalplastic flow mechanism. Creep has been detected experimentally (Robertson, 1960) in dry chalk samples compressed hydrostatically. Calcareous sediments will deform in crystalplastic flow at low temperatures unlike terrigenous clastics consisting of quartz grains. Pressures high enough to cause crystalplastic flow in quartz sandstones usually result in grain crushing and cataclastic flow leading to plastic deformation (Zhang et al, 1990). Zhang et al (1990) did not report detectable creep in their triaxial compression tests on Berea sandstone.

To describe creep and viscoelasticity, many phenomenological models have been developed (e.g., Bourbie et al, 1987). These consist of idealized mechanical components to represent linear viscosity and elasticity. The standard linear solid model is a simple example of an idealized viscoelastic material consisting of two springs and dashpot. This model, like all viscoelastic models, will have a stiff response for high frequency strains, and a compliant response for low frequency strains depending on the relative magnitudes of the elastic and viscous part of the modulus. Given the deformation response to a ramp force, the values of viscosity and elasticity can be extracted from the creep time constants. These parameters will roughly describe the mechanical behavior of the rock. By finding the frequency dependent moduli of the standard linear solid, one can estimate the frequency dependence of the rock sample.

EXPERIMENTAL PROCEDURE

In paper G6 we describe stress cycles on a sample of dry turbiditic sand in a pressure vessel. During one of the many runs, a series of axial compressions under confinement were performed. In all of the experiments, we observed creep during hydrostatic loading and axial loading. To keep this creep from superimposing itself on the unloading response of the rock during stress cycling, we let the samples sit for 5 to 10 hours after reaching peak stress. During these waiting periods, we recorded the strain on the samples. These were basically creep curves resulting from a constant stress rate ramp. The ramp was 4 MPa in 1 hour, under confining pressure varying from 10 to 25 MPa.

Our tests also included three creep tests on Ottawa sand samples. The first sample was clean Ottawa sand. The second sample was tested with 15% dry Montmorillonite clay mixed into the sand. The third sample was a 15% Montmorillonite clay sample with the clay premoistened, then air dried before compression. These tests investigated the possibility of clay content being responsible for creep.

RESULTS AND ANALYSIS

Data for the creep tests is shown below in Figure 1. A 4 MPa axial loading ramp test on a sample of Upper Terminal turbidite under 20 MPa of confining stress is shown. For approximately 5 hours, the sample was allowed to creep. The axial stress of 4 MPa and confining pressure of 20 MPa was maintained while the sample was monitored. The data shown shows the transient behavior after the pressure is shut in at $t=0$. We observed creep in hydrostatic tests as well (Figs. 1b, 1c). These tests show less creep than the axial case. They were performed under lower stresses and they had no shear stress. The clean Ottawa sand sample did not creep, nor did the mixture of dry Montmorillonite clay and Ottawa sand. The mixture of moistened then air dried Montmorillonite clay and Ottawa sand did show a creeping behavior (Fig. 1c) with approximately the same amount of strain as the hydrostatically tested Upper Terminal zone turbidite. The two Figures 1b and 1c show approximately the same amount of strain although over different times;

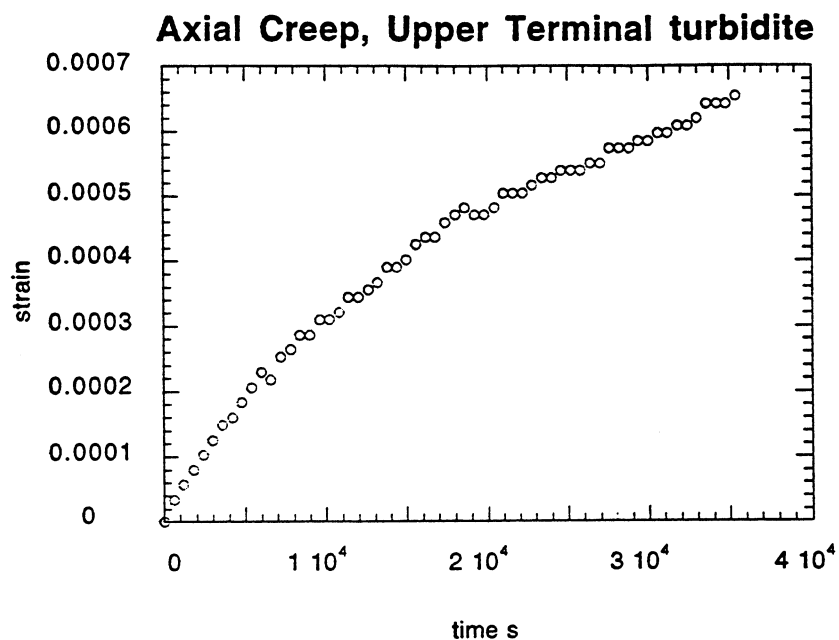


Figure 1a: Strain vs. time after loading to 4 MPa of axial stress in an Upper Terminal zone turbidite. The sample was under 20 MPa of confining pressure.

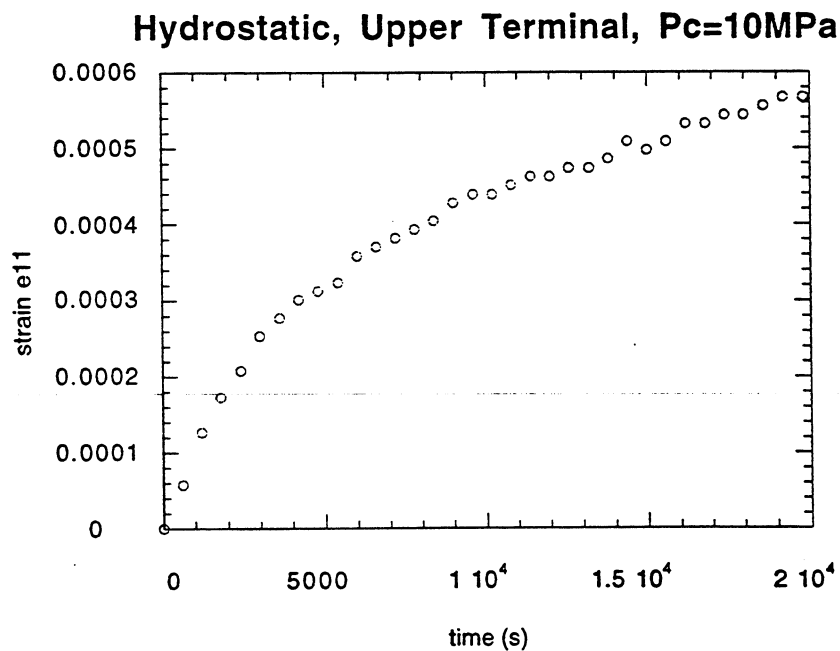


Figure 1b: Strain vs. time after loading to 10 MPa of confining stress in an Upper Terminal zone turbidite. Note the creeping is the same order of magnitude as in the axial case.

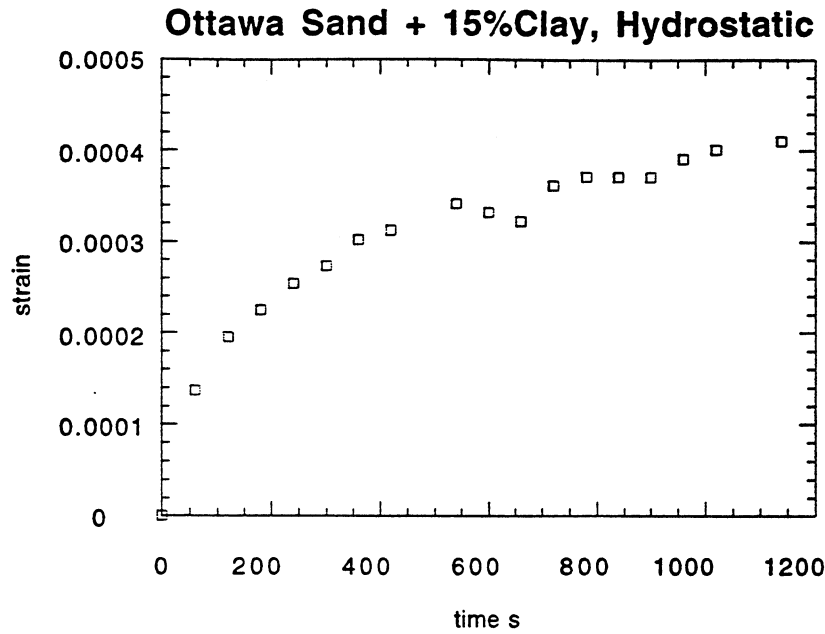


Figure 1c: Strain vs. time after loading to 10 MPa of confining stress on an Ottawa sand sample mixed with 10% Montmorillonite clay. Although clean Ottawa samples showed no creep, adding Montmorillonite clay to a sample of Ottawa sand induced creep.

Using the standard linear solid viscosity model (Fig. 2), we attempted to modeled the mechanical behavior of our rock sample . The model is a combination of Hookean springs and a Newtonian dashpot. The relative values of these components determines the crossover point from high to low frequency behavior.

A simple differential equation can be written to describe the behavior of the solid in one dimension (see equation 1):

$$\eta \dot{\sigma}_{11} + (E_1 + E_2) \sigma_{11} = E_2 (\eta \dot{\epsilon}_{11} + E_1 \epsilon_{11}). \quad (1)$$

where η is the dashpot, σ the stress, ϵ the axial strain, and E_1 and E_2 the spring stiffnesses. The free parameters are the viscosity, and two spring constants.

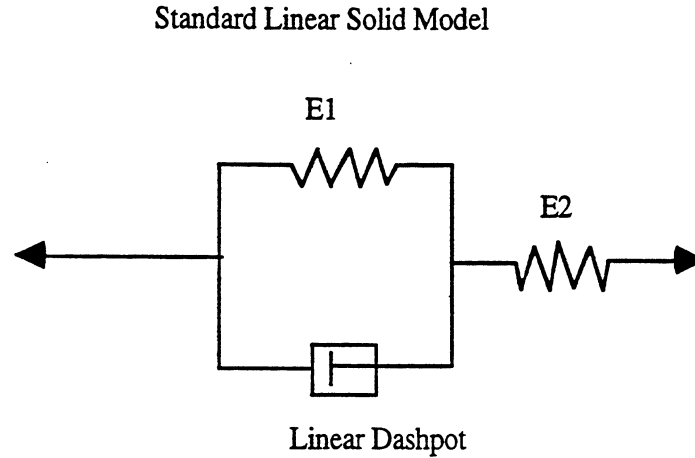


Figure 2: The standard linear solid viscoelasticity model. The springs are Hookean and the dashpot is Newtonian.

Examining the behavior of these functions can relate the stress, strain, viscosity, elasticity, stress rate, and time for a model rock undergoing compression. We used Matlab, to calculate the creeping response given a 1 hour loading ramp (Fig. 3). The high frequency limit was calculated from the wave propagation experiments at high pressure (Paper G6). Initial estimates of the high and low frequency limits of the frame modulus $E1$ and were determined from lab data (Paper G6). The low frequency limit was approximated from the static bulk modulus and using the measured dynamic Poisson's ratio as .25. The data was fit by adjusting the viscosity. The raw axial data in Figure 1a was fit with the standard linear solid model to determine the parameters shown in table 1 resulting in Figure 3.

| | |
|------------------|----------|
| Viscosity (Pa.s) | 1.85E+13 |
| Spring 1 (Pa) | 2.5E+9 |
| Spring 2 (Pa) | 1.0E+10 |

Table 1: Parameters determined by fitting the axial loading data.

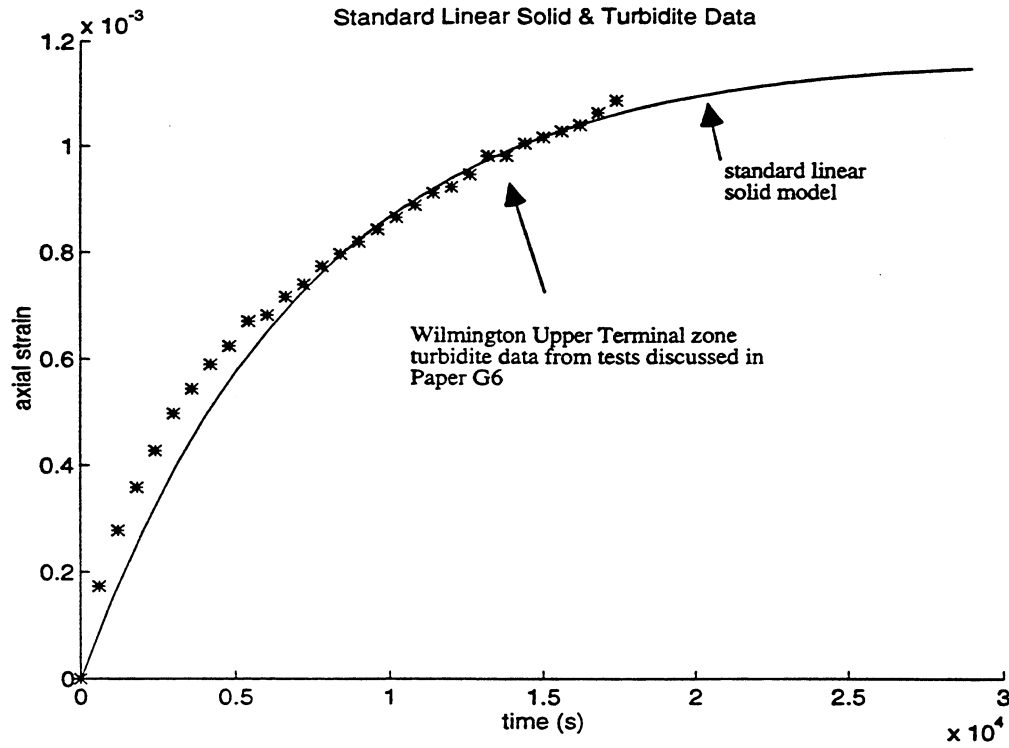


Figure 3: The fit of the axial loading data to the model.

After determining the model parameters, it is possible to determine the system's frequency dependence. The standard linear solid has a complex modulus of the form,

$$M(\omega) = \frac{E_2(E_1 + i\omega\eta)}{E_1 + E_2 + i\omega\eta} \quad (2)$$

By taking the magnitude of this complex number and plotting it as a function of frequency, we can determine the dispersive behavior of the system. As end members, the sample has the elasticity of the two springs in series at low frequency, and the second spring at high frequency.

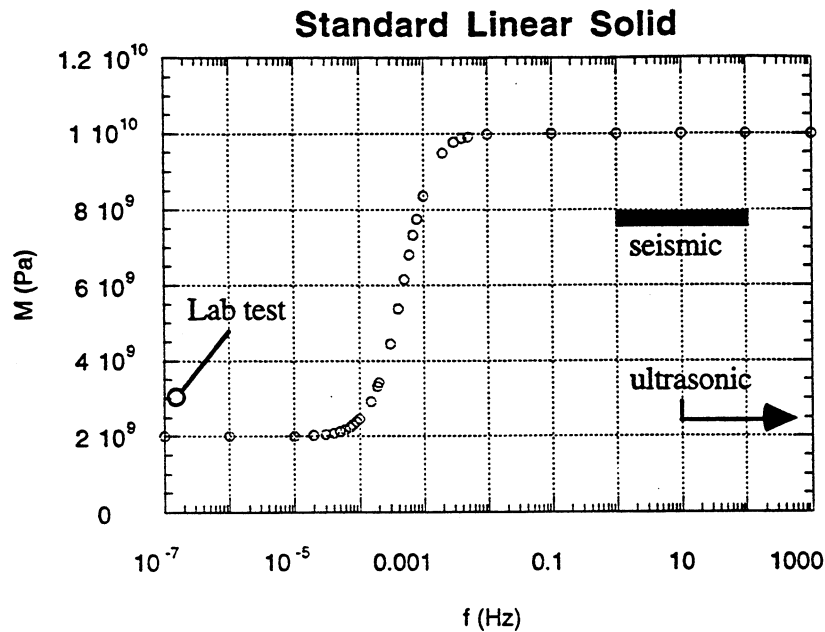


Figure 4: The magnitude of the modulus as a function of frequency. Note the low crossover point indicative of a highly viscous component in a compliant solid.

As expected from viscoelasticity, the model rock stiffens with loading rate. Also, there is a high frequency limit associated with high loading rates where the spring constant approaches the stiffness of spring #2.

DISCUSSION

The viscoelastic response of the sands tested may be an explanation for the relationship between static and dynamic modulus. The dispersion curve indicated that the sample was very viscous. Viscoelasticity is unusual in a dry sand, since we expect to find it associated with the discharge of pore fluids. We have several hypotheses, (1) microcracking could be leading to cataclastic flow of the grains, (2) strain amplitude differences between the high pressure loading of the sample and the ultrasonic measurement gives different moduli due to material nonlinearity, or (3) clay and mica between the grains may be affecting the overall modulus measurement for large deformation. Given the amount of mechanical and microstructural evidence, hypothesis (3) appears to be the most likely mechanism.

Time dependent microcracking has been studied in fault mechanics to explain aseismic creep on faults (Costin, 1987). We may be looking at grain crushing and

cataclastic flow (Zhang et al, 1990). This is improbable because cataclasis usually occurs at much higher pressures than we have gone to in the lab (Zhang et al, 1990). Grain angularity may get around this since stress concentrations can be quite large on a pointlike contact. However, at the temperatures and pressures of the experiment, this seems improbable.

Strain amplitude and sample nonlinearity is another possible reason for dispersion. The samples we deformed are nonlinear in both hydrostatic loading and triaxial loading. If the sample has a very nonlinear stress vs. strain response, a large amplitude strain may give a lower stiffness measurement since we are trying to describe the behavior with a single constant. The ultrasonic measurement is a small deformation that gives a more linear measurement since no inelastic deformation occurs. Tutuncu et al (1995) explained dispersive behavior of cemented sandstones with differences in strain amplitude. However, although this explains the large difference between static and dynamic modulus, it leaves the creeping behavior unaddressed.

Soft intragranular materials under high pressures could give rise to time dependent deformation. Analysis of thin sections reveals that of the samples indicated that much of the 20% mica fraction was placed between stronger grains of quartz, feldspar, and lithic particles. The mica was deformed during the natural consolidation process along the quartz boundaries and could dramatically affect the mechanical properties of the rock. Small amounts of clay in the matrix could give rise to a similar mechanical behavior, as suggested by the creep which occurred in the 15% Montmorillonite clay and Ottawa sand mixture, that exhibited creeping behavior. This seems to favor this mechanism as an explanation for the creeping behavior as well as the dispersion.

The relative values chosen for the viscosity and the elasticities in the model strongly suggest that the clay and mica hypothesis is correct. At low frequency, the turbidite is compliant, and very viscous. A well cemented sandstone saturated with water would represent a stiff set of springs and a very inviscid dashpot. A stiff rock matrix, represented by spring E1 in the model, combined with a smaller the viscous component, will result in less dispersion than a compliant matrix with the same viscous component. This was seen in Winkler (1983) where saturated experiments on fused glass beads showed less dispersion than saturated experiments on Massillon sandstone because of the glass beads' higher matrix stiffness. The turbidite dispersion results imply that the opposite is also true. If the system is very compliant, represented by a weak spring E1, and highly viscous, represented by a large η , low frequency measurements such as creep tests will be dominated by the dashpot, while high frequency tests will be dominated by the spring E2 since the dashpot will be locked. This may explain the differences between the turbidite

and Ottawa sand. It's possible that the micas and clays contribute the highly viscous term which dominates at low frequencies since the unconsolidated matrix is compliant. The Ottawa sand, although compliant, has no viscous mechanism and the high and low frequency elasticities E_1 and E_2 add in series resulting in a nearly linear response with no dispersion.

This phenomenological model along with the evidence from clay mixture tests and thin sections suggests that the intragranular clay and mica hypothesis is potentially a viable mechanism for dispersion in these samples.

CONCLUSION

The creep response of our Upper Terminal zone turbidite provides information about the mechanical behavior of the sample at high and low frequency. The experimental results suggested that the mica and clay content between the hard quartz grains may be the mechanism responsible for viscoelasticity in dry sand. By modeling the mechanical behavior with a series of compliant springs to represent the poorly consolidated grains, and a very viscous dashpot, to represent the intragranular clays and micas, we determined the frequency dependent modulus of the rock. The combination of experimental data, thin section data, and modeling results, favor the soft intragranular mica and clay hypothesis as an explanation for the highly dispersive behavior.

ACKNOWLEDGMENTS

Special thanks to Tidelands Oil and The Department of Energy who funded this research. Also, thanks to New England Research, who constructed the pressure vessel and acquisition/control system for the apparatus. Thanks to Don Lowe of the Department of Geology, Stanford University for his help on the thin section analysis.

REFERENCES

- Biot, M.A., 1956, "Theory of propagation of elastic waves in a fluid saturated porous solid." II. Higher-frequency range, *J. Acoust. Soc. Amer.*, **28**, 168-178.
- Bourbie, T., Coussy, O. and Zinser, B., 1987, "Acoustics of porous media", Gulf Publishing Company.
- Costin, L.S. 1987, "Time -dependent deformation and failure", in "Fracture Mechanics of Rock", edited by B.K. Atkinson, Academic Press.
- Dvorkin, J. and Nur, A., 1993, Dynamic poroelasticity: A unified model with the squirt and the Biot mechanism: *Geophysics*, **58**, 524-533.
- El Refai, W.T.H, and Hsu, J.R., "Creep deformation of clays," *Proc. ASCE J. Soil tech. Engng. Div.*, **104**, GT, 61-76, 1978.
- Mavko, G. and Jizba, D., 1991, "Estimating grain-scale fluid effects on velocity dispersion in rocks," *Geophysics*, **56**, 1940-1949.
- Mavko, G., and A. Nur, 1979, "Wave attenuation in partially saturated rocks", *Geophysics*, **44**, p.161-178.
- Robertson, E.C., 1965) Robertson, Eugene C., et al. "Experimental consolidation of calcium carbonate sediment." 1962. U. S. GEOLOGICAL SURVEY PROFESSIONAL PAPER ; P 0350, p. 82-83.
- Tutuncu A.N.; Podio A.L.; Sharma M.M; "Nonlinear Viscoelastic Behavior of Sedimentary Rocks: I. Effect of Frequency", submitted to *Geophysics*, February 1995
- Terzaghi, K., 1936, "The stability of slopes of natural clay," *Proc. 1st Int. Conf. Soil Mech. Found. Engng.*, Cambridge, Mass., **1**, 161-165.
- Winkler, K.W., 1983, Frequency dependent ultrasonic velocities of high porosity sandstones, *Journal of Geophysical Research*, **88**, 9493-9499.
- Zhang, J., Wong, T.F., Davis, D.M., 1990, "High pressure embrittlement and shear-enhanced compaction of Berea Sandstone; acoustic emission measurement and microstructural observation", *Rock mechanics; contributions and challenges; proceedings of the 31st U.S. symposium*; Vol. **31**, p. 653-660.

PAPER G6**A COMPARISON OF DYNAMIC AND STATIC MODULI IN
UNCONSOLIDATED RESERVOIR ROCKS FROM THE WILMINGTON
FIELD, CALIFORNIA****Carl T. Chang****Dan Moos****Mark D. Zoback***Stanford Borehole Geophysics Laboratory***ABSTRACT**

Measurements of the elastic properties of unconsolidated sand samples recovered from the Wilmington field, Long Beach, California have been made at pressures simulating in situ conditions. Dry samples were tested under hydrostatic loading to determine accurate values of the frame moduli for a related study on fluid detection from logs (see Paper G3). Dynamic shear and bulk moduli were calculated from P- and S-wave velocities determined during loading by pulse transmission. Both static and dynamic bulk moduli increase with pressure. However the dynamic bulk modulus is consistently three times higher than static bulk modulus. In the same experimental apparatus, a sample of dry Ottawa sand showed no difference between static and dynamic modulus suggesting that constituents present in the turbidite and absent in the clean sand, such as micas and clays, were responsible for the frequency dependent moduli.

INTRODUCTION

In theory, static and dynamic modulus should be the same for an elastic material. This is observed in crystalline materials where both static deformations and deformation arising from wave propagation are small. However, this is not the case in sedimentary rocks. For example, in cemented sandstone, dispersion has been observed and attributed to the effects of fluid saturation in the pore space (Mavko & Nur, 1979). Wave attenuation and dispersion in saturated sandstone has been studied and documented (Murphy & Winkler 1982). Using simultaneous ultrasonic measurements and triaxial stress cycling, Tutuncu et al (1995) determined that apparent dispersion can also be a result of differences in strain amplitude between high and low frequency measurements.

Previous work on Upper Terminal zone turbidites from the Wilmington field, CA demonstrated that loading bulk moduli were more than six times smaller than moduli derived from simultaneous pulse transmission experiments. This is a consequence of irreversible pore compaction during loading, which was a result of plastic deformation associated with pore collapse (as suggested by Han, 1995, pers. comm.).

To compare dynamic and static moduli in a sample that yields plastically requires measurement of static modulus during unloading. Additionally, by simultaneously conducting pulse transmission experiments (e.g. Tutuncu et al, 1995), we can determine both the high-frequency small-strain modulus and the low-frequency large-strain modulus during elastic and elastoplastic limbs of each loading cycle. This isolates the loading and unloading moduli on two legs of the loading curve and yields a more realistic comparison of static and dynamic moduli.

EXPERIMENTAL PROCEDURE

As in last years' investigation of unconsolidated rock, core samples were obtained from the Wilmington field, Long Beach, California in well UP941b from a depth of 3233 feet. The samples were a fine grained turbidite sand from the Upper Terminal zone. Thin section analysis indicated that the sample consisted of approximately 20% quartz, 20% feldspar, 20% crushed metamorphic rocks, 20% mica, and 10% clay. The poorly sorted grains are highly angular with a mean grain size of 300 μm . After plunge cutting at room temperature with steel tubing we extruded the samples into soft polyolefin jacketing. The jacketed specimen was 1" in diameter and 2" long. Before testing, residual heavy oil was removed from the samples by flushing first with mineral spirits and then with air to dry the porespace. The samples were then wired to a transducer stack and placed in a pressure vessel for testing under room-dry conditions.

Cyclic loading was performed in the following manner (see Figure 1): the sample was initially pressurized to 10 MPa at a loading rate of $10^{-7}/\text{s}$ (the first loading leg). It was then allowed to sit for 5 hours to allow transient creep to subside (the creeping leg). Then the pressure was lowered to 5 MPa at $10^{-8}/\text{s}$ (the unloading leg). Similar cycles were repeated, with each cycle reaching a maximum confining pressure 10 MPa higher than the previous cycle, to a maximum confining pressure of 30 MPa. Simultaneous travel time measurements were made by propagating P- and S- waves along the axis of the cylinder using 1MHz quartz crystals as shown in Fig. 1. An automated data acquisition system recorded hydrostatic stress and axial deformation as well as the full waveforms transmitted through the sample. A sample of dry unsorted Ottawa sand was tested in a similar fashion.

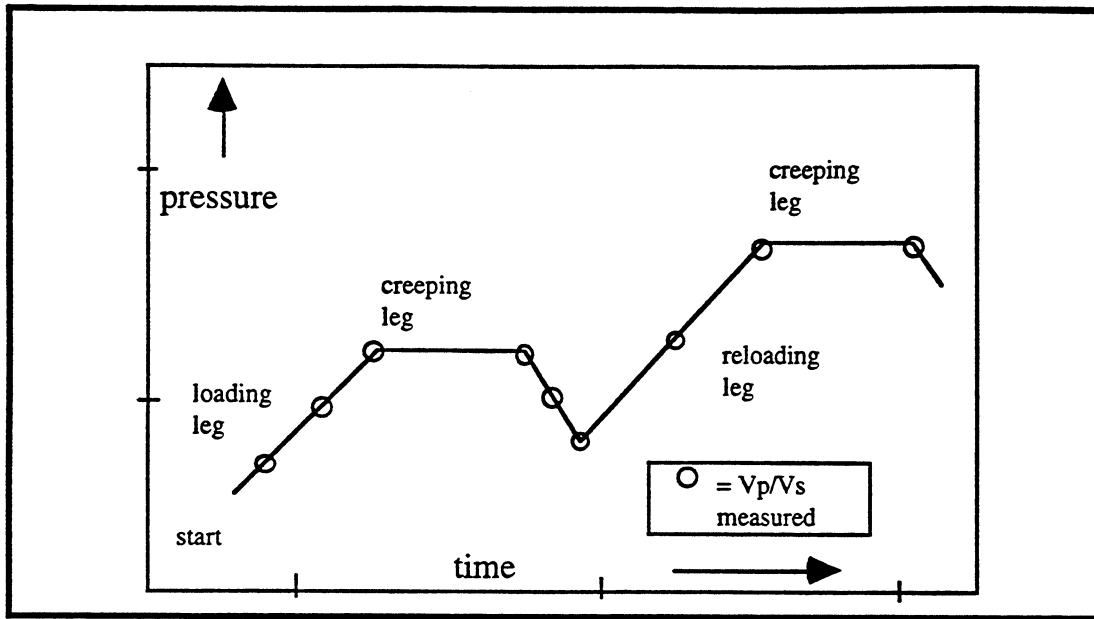


Figure 1: The loading process showing pressure vs. time. First the sample is loaded using a constant stress rate to a nominal pressure. The pressure is shut in and the sample is allowed to creep. The sample is then unloaded to an intermediate pressure then reloaded linearly to the next creeping leg.

RESULTS

Figure 2 shows the response of the turbidite and of the Ottawa sand to the loading history outlined above. The turbidite (Fig. 2a) shows a highly elastoplastic mechanical response; the difference in slope between a loading leg and the following unloading leg is due to irreversible plastic strain during loading. As in soil tests, the sample reloaded along the unloading curve until the previous maximum pressure was achieved, at which point the sample begins to yield plastically again and the loading curve continues along its previous path. When the loading was paused at the top of each cycle, the sample would creep for approximately 5 hours (see Paper G7). Therefore, we held the pressure constant before unloading the sample to allow transient creep to abate.

In the same experimental apparatus, the Ottawa sand sample showed a significantly different mechanical behavior. Although this sample had approximately the same mean grainsize, it behaved almost purely elastically, unlike the Upper Terminal zone turbidite. This is seen in the loading and unloading paths in Fig. 2b that nearly superimpose upon one another. The loading slope is greater than that of the turbidite sample, but the unloading slope is smaller. Nor did the Ottawa sand sample exhibit creeping behavior. Unfortunately, the return path from 30 MPa to 0 MPa wasn't recovered because of an acquisition failure towards the end of the test.

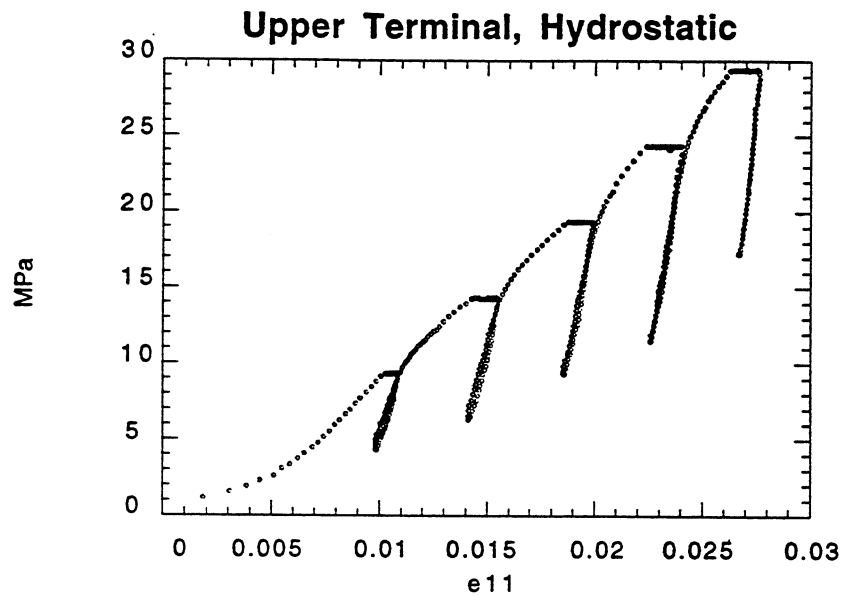


Figure 2a: The stress vs. strain response of the turbidite under hydrostatic loading. The curve shows a highly plastic response. Note that the unloading cycles have a higher slope than the loading cycles, yet, the successive loading cycle follows the previous loading curve.

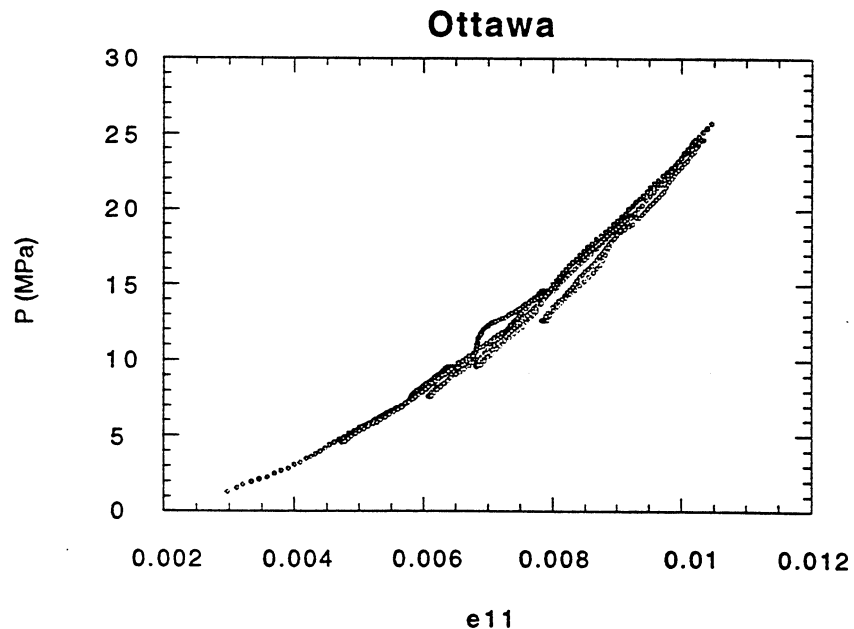


Figure 2b: The stress vs. strain curve for a similarly tested sample of dry Ottawa sand with approximately the same mean grain size, shows a significantly different elastic response. The final unloading curve is not shown here because of an acquisition failure at the end of the experiment.

Figures 3 and 4 show P - and S -wave velocities calculated from travel times of axially propagated waves and length corrected for strain. The velocities are consistent with results measured on other unconsolidated sand samples (Dominico, 1977, Estes et al, 1994). As with all sands, the velocity increases monotonically with pressure. Assuming linearity and isotropy, we calculated the dynamic elastic moduli for these velocities correcting for the deformed density from the volumetric strain. Velocity values are shown for the turbidite and Ottawa sand in Figure 5. The bulk moduli measured from velocity show the same increasing trend with increasing pressure. By calculating the slopes of the stress vs. strain curve during the unloading cycle exerted by the confining pressure we determined the static compressibility of the matrix. This value is plotted along with the dynamic moduli in Figures 6 and 7 for Upper Terminal turbidite and Ottawa sand respectively.

The dynamic Poisson's ratio is easily calculated from the Upper Terminal velocities (Figure 8). The value of 0.25 measured above about 5 Mpa is quite large, in comparison with data from clean sands reported in previous SRB volumes.

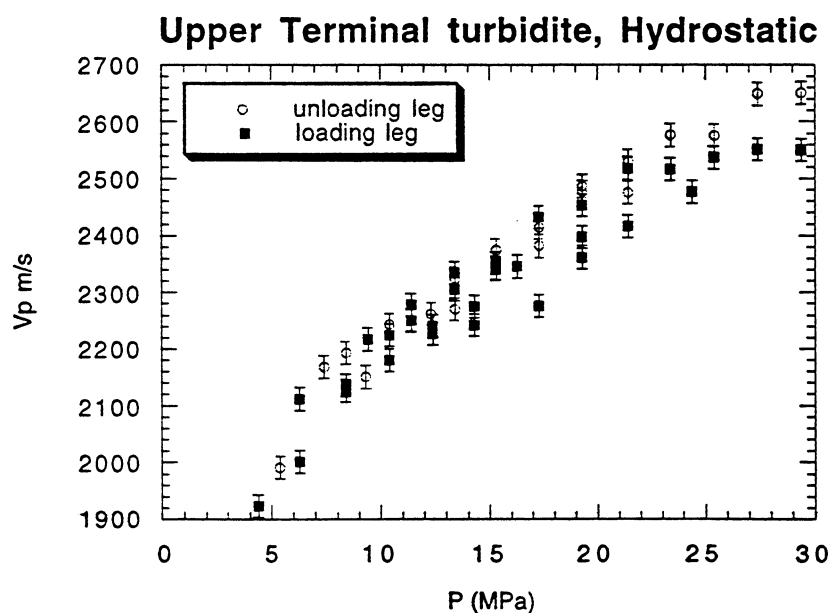


Figure 3: P- wave velocities in the turbidite calculated from the travel time along the axis of the sample corrected for axial strain.

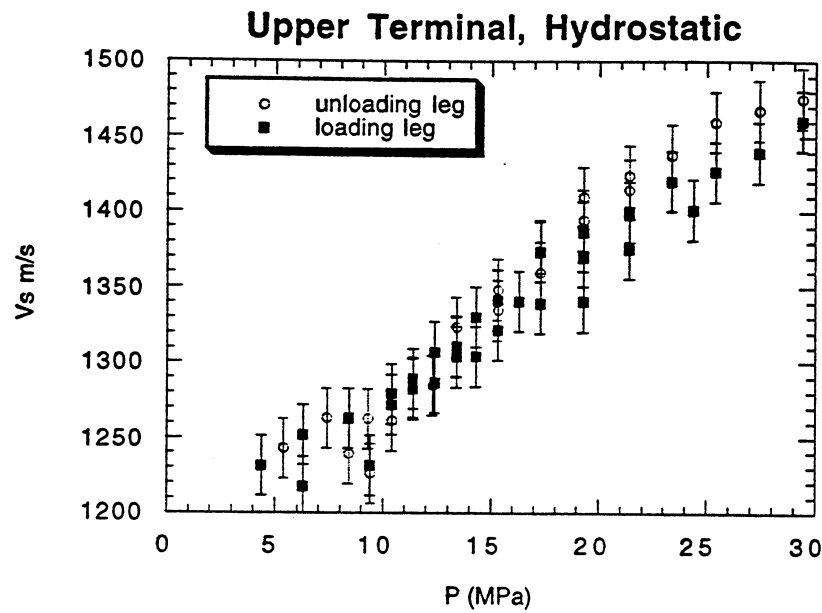


Figure 4: S-wave velocities in the in the turbidite calculated from the travel time along the axis of the sample corrected for axial strain.

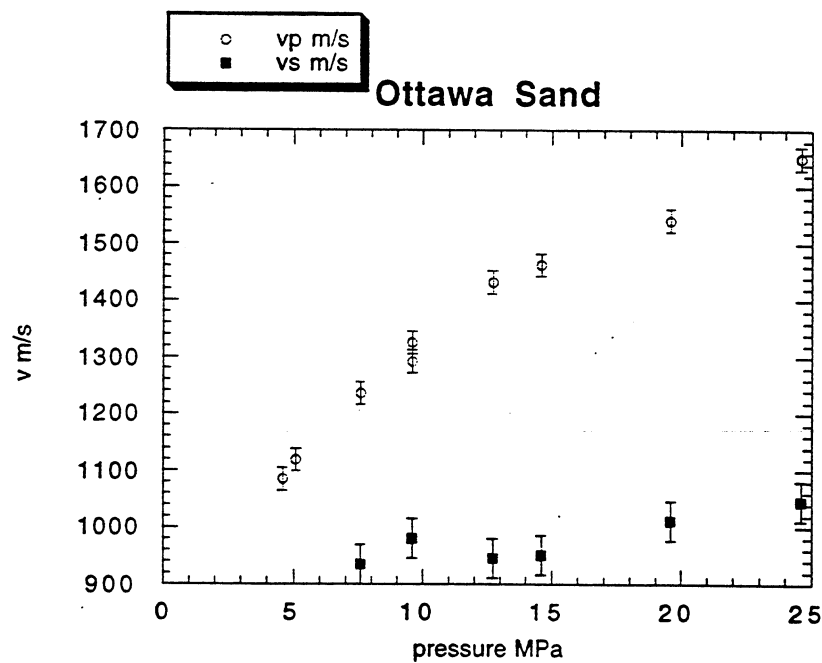


Figure 5: P- and S- wave velocities for Ottawa sand tested in the same apparatus. Data was only collected on the loading legs.

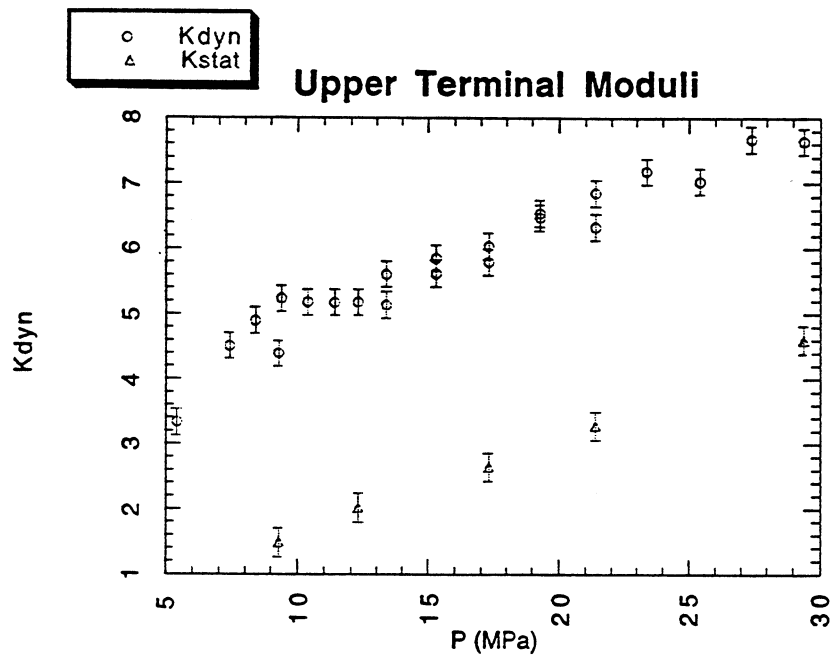


Figure 6: Bulk moduli of the turbidite sample. The static modulus (Kstat) shows the same increasing trend with pressure that the dynamic moduli (Kdyn) show, however it is significantly smaller than bulk modulus determined from wave propagation.

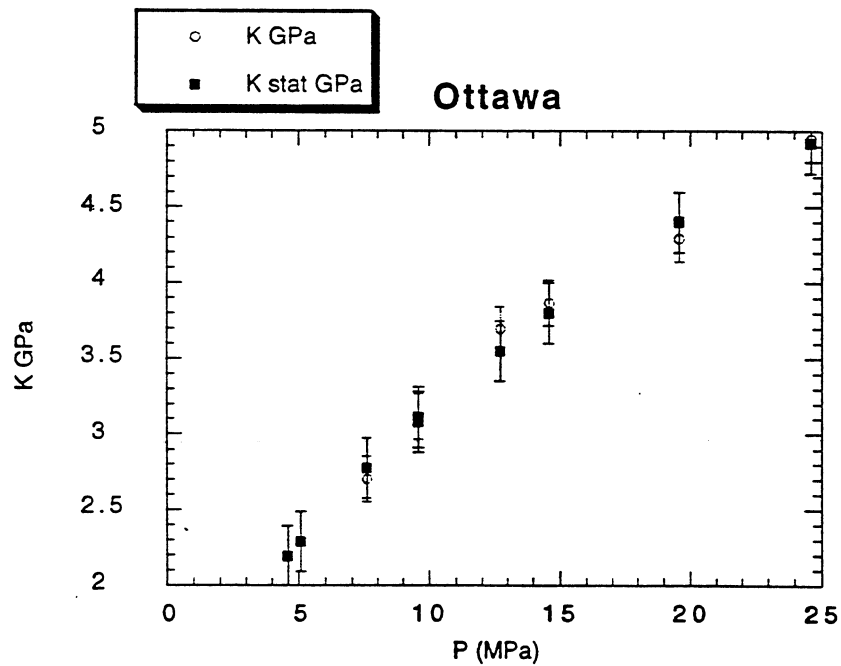


Figure 7: The Ottawa sand static moduli (Kstat) and dynamic moduli (Kdyn). Note the strong correspondence between the two.

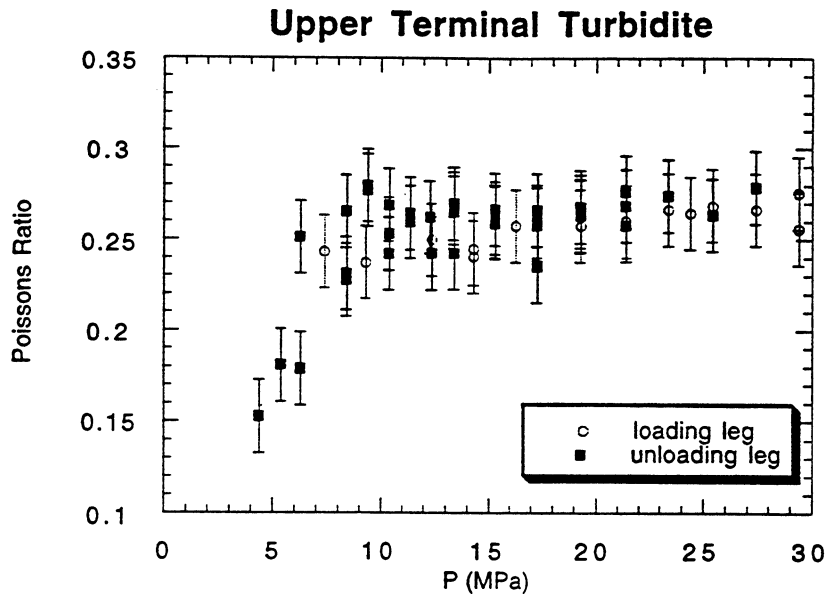


Figure 8: The Poisson's ratio of the turbidite. The measurement shows pressure sensitivity at low pressures.

DISCUSSION AND CONCLUSIONS

The Ottawa sand sample and the Upper Terminal zone turbidite have similar grain size and were treated similarly during sample preparation. However, one major difference is the presence in the turbidite of more than 10% by volume clay and as much as 20% by volume mica. To investigate this, we prepared two new samples of Ottawa sand, each with 15% by volume montmorillonite. The results of creep tests on these materials discussed in Chang et al. (Paper G7) demonstrate that the difference in behavior between the turbidite and clean Ottawa sand during testing can be explained by the presence of wetted clays and/or mica in the turbidite.

Differences between loading and unloading modulus of the turbidite are a consequence of irreversible compaction during loading, a behavior which can be appropriately modeled using elastoplasticity. However, differences between static unloading moduli and dynamic moduli of 300% persist. These can be explained by viscoelasticity associated with the clays and/or micas. As discussed in Paper G7, the static unloading and dynamic moduli were appropriate to describe the creep response of the turbidite. Using the viscosity required to fit the creep curve, the transition from low-frequency to high-frequency behavior occurs at a frequency which is several orders of magnitude less than seismic. Thus, it is appropriate to use the ultrasonic measurements of

dry modulus as inputs to Gassmann to predict the elastic properties of fluid-saturated sands in situ in the Wilmington field.

ACKNOWLEDGMENTS

Special thanks to Tidelands Oil and The Department of Energy who funded this research. Also, thanks to New England Research, who constructed the pressure vessel and acquisition/control system for the apparatus. And finally, thanks to Don Lowe of The Geology Department, Stanford University, for helping with the thin section analysis.

REFERENCES

- Chang C., Moos D., Zoback M.D. "Mechanical Properties of unconsolidated materials", SRB 95 Annual Report, Vol. 58, Paper A5.
- Bourbie, T., Coussy, O. and Zinser, B., 1987, "Acoustics of porous media", Gulf Publishing Company
- Dominico, S. N.; "Elastic properties of unconsolidated porous sand reservoirs", 1977, Geophysics, Vol. 43, 7, p. 1339-1368.
- Estes, C.A., Mavko, G., Yin, H., Cadoret, T.; "Measurements of velocity, porosity and permeability on unconsolidated granular materials", 1994, SRB Annual Report, Paper G1.
- Han, D. H., personal communication, 1995.
- Karig, D.E.; "Reconsolidation tests and sonic velocity measurements of clay-rich sediments from the Nankai Trough," Proceedings of the Ocean Drilling Program, Scientific Results, Vol. 131.
- Mavko, G., and A. Nur, "Wave attenuation in partially saturated rocks", Geophysics, 44, 161-178, 1979
- Murphy, W. F., III, Winkler, K.W.; "Acoustic relaxation in sedimentary rocks; dependence on grain contacts and fluid saturation." March 1986. (GEOPHYSICS ; Vol. 51, No. 3, p. 757-766)
- Tutuncu A.N.; Podio A.L.; Sharma M.M; "Nonlinear Viscoelastic Behavior of Sedimentary Rocks: I. Effect of Frequency", submitted to Geophysics, February 1995
- Winkler, K.W.; "Frequency dependent ultrasonic properties of rocks", GEOPHYSICS; VOL. 88, NO. B11, p. 9493-9499, 1983.

PAPER H6**HYDROCARBON SATURATION DETERMINATION
FROM SONIC LOG DATA****Daniel Moos***Stanford Rock and Borehole Geophysics Project***Andrew Hooks***Magnetic Pulse, Inc.***Scott Walker***Tidelands Oil Production Company***ABSTRACT**

Theoretical relationships, confirmed by laboratory and field data, suggest that hydrocarbon-bearing rocks in situ can be differentiated from rocks containing brines using sonic velocity measurements. A project to test this technique has been undertaken in the Wilmington Field, California, with co-funding from the Department of Energy (DOE cooperative agreement no. DE-FC22-95BC14934).

Results from M-499 (selectively completed in the Upper Terminal Zone) and 167-W (a Lower Terminal Zone injector) demonstrate that the theoretically predicted effects can be observed. Zones with producible oil can be differentiated from those which are watered out using acoustic logs recorded through casing.

THE WILMINGTON FIELD

The Wilmington field is located within a NW-SE trending faulted anticline beneath and immediately offshore of Long Beach, CA (Figure 1). The first successful well was drilled in 1936. As of 1967, more than 1.2 bbls of oil and 840 Tcf gas had been produced, and it was believed that more than 1.8 bbls of oil still remained. Initial production was enhanced by a waterflood started in the 1950's primarily to mitigate surface subsidence which had reached more than 29 feet in the center of the bowl directly overlying the region of greatest production. Injection wells are located at the margins of the field, and production continues from the center.

Production at Wilmington is from a thick sequence of clastic slope sediments (unconsolidated, low maturity, turbiditic arenites and clean arenites with porosities exceeding 25% and permeabilities of 100's of millidarcys, interlayered with sandy clays (wackes) containing 50% or more detrital smectite). The producing horizons lie between depths of 2350 and about 6000 feet. The hydrocarbons produced at Wilmington range from API gravity 12 (Tar zone) to API gravity 18-19 (Ranger and Upper Terminal Zones) to API gravity 27 (Lower Terminal). API gravities as high as 30 are produced from deeper sections of the field (the Union Pacific, Ford, and 238 zones).

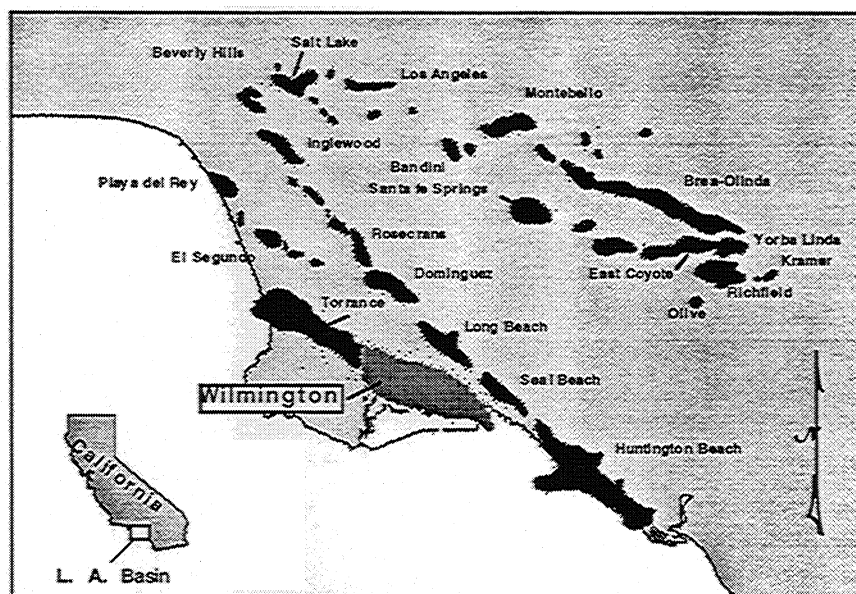


Figure 1: Location map, showing the Wilmington Field and other oil fields within the Los Angeles Basin (after Mayuga, (Mayuga, 1968)).

THEORETICAL BASIS OF THE SONIC DETECTION TECHNIQUE

Generally, when a rock is loaded under an increment of compression, such as from a passing seismic wave, an increment of pore pressure change is induced, which resists the compression and therefore stiffens the rock. The low-frequency Gassmann (1951) - Biot (1956) theory predicts the resulting increase in effective bulk modulus of the saturated rock. Gassmann predicted no change for the isotropic shear modulus with saturation. The Gassmann-Biot relation is valid only at sufficiently low frequencies such that the induced pore pressure is equilibrated throughout the pore space (i.e., that there is sufficient time for the pore fluid to flow and eliminate wave-induced pore pressure gradients). Laboratory measurements are under way to investigate whether this will be important at logging frequencies (Chang et al., this volume).

The ability to detect hydrocarbons using elastic waves depends both on the amount by which hydrocarbon properties differ from those of brines and the degree to which those properties control the velocities of the saturated rock. Several factors influence the properties of fluids at reservoir conditions. In general, density, bulk modulus and viscosity all decrease with increasing API number (decreasing density) and temperature and increase slightly with increasing pressure. Gas in solution has a large effect, even in comparison to that of temperature, in reducing density and bulk modulus. Based on equations presented in Batzle and Wang (1992), live oils at reservoir conditions have significantly lower bulk moduli and densities than those of brine. And, the relatively low frame modulus (high pore compliance) of Wilmington reservoir rocks suggests that they will be quite sensitive to the properties of fluid saturants (see Fig. 3, Moos et al., this volume).

PREVIOUS RESULTS

Previously, theoretical models using values of fluid and formation properties typical of the Miocene-age turbidites within the target interval confirmed that it should be possible to differentiate between hydrocarbon and non-hydrocarbon bearing sands in this field using compressional and shear wave sonic velocity logs (Moos, 1995). And, results in a newly drilled well demonstrated that it was possible to record shear and compressional wave velocities through casing. Shear velocities recorded through casing in the frequency band between 0.8 and 2.4 kHz were virtually identical to the open-hole values. However, in the frequency band between 4 and 8 kHz, compressional velocities calculated using cased hole data were slightly less than those calculated using open-hole data, and open-hole velocities computed using data filtered to isolate energy propagating at 2.5 to 3.5 kHz were slightly greater than those calculated using the open-hole data at higher frequency (Moos, et al., 1995). Porosity estimated using an empirical relationship between shear velocity and porosity was similar to that determined from a density-neutron crossplot. Estimates of saturation were qualitatively similar to conventional (Archie's Law) values. The well was completed by selectively perforating zones with high Archie's Law predicted oil saturations, and outperformed adjacent wells completed using slotted liners and/or gravel packings.

To date six wells have been logged through casing, using several versions of the MPI XACT sonic logging tool. Two of these were also logged using the Schlumberger DSI tool. In M-499 and two of the newly logged wells, Schlumberger USI logs were run to investigate casing bond. A standard bond log was also run in M-499. The oldest wells were drilled in the 1940's. Deviations ranged from less than 2° to more than 40°. Casing diameters were between 6" and 8".

Table I: Summary of hole characteristics.

| Hole | Depth* | Deviation | Year Drilled | Well Type |
|--------------------|---------|-----------|--------------|-----------|
| M-499 | 2.8-3.7 | 43° | 1993 | Prospect |
| 167-W [†] | 2.5-4.5 | 30° | 1983 | Injector |
| FY-67 | 1.6-3.7 | 17° | 1948 | Injector |
| Y-63 | 1.6-3.2 | 17° | 1948 | Prospect |
| X-32 | 3.0-5.6 | - | 1946 | Prospect |
| J-15 | 1.2-2.9 | vertical | 1942 | Prospect |

*kft

[†]Steel casing extended to 4080 ft, below which fiberglass liner was installed and perforated to allow injection into selected zones.

Although compressional velocities have been determined in all but one case, shear-wave velocities have been obtained in only two of the six wells. In determining whether these logs actually measure the shear wave, independent recordings of arrivals on opposite sides of the tool are essential. Based on the results to date, the two most important determinants of success are the age of the well and the difference between shear-wave and tube-wave velocities. Neither standard cement bond logs nor bond estimates derived using acoustic reflections from casing could be used to unambiguously predict whether shear-wave logs could be obtained. Nor did the angle of deviation, as M-499, for which excellent data were obtained, was deviated 43°, and J-15, for which no shear-wave velocities could be determined, was vertical.

DATA

Data are now available from two wells to test whether producible hydrocarbons can be detected acoustically in the Wilmington Field. The first well, M-499, was drilled and selectively completed in the Upper Terminal Zone over the depth interval 3120 to 3540 feet (log depths are not corrected to true vertical depth). Excellent cased-hole compressional and shear velocities were obtained in this well (Moos, et al., 1995, Moos, 1995). The second well, 167-W, was drilled in 1984 and cased to 4080 feet. A fiberglass liner was placed below that depth and selectively perforated to allow injection into permeable sands of the Lower Terminal Zone over the depth interval 4200 to 4680 feet.

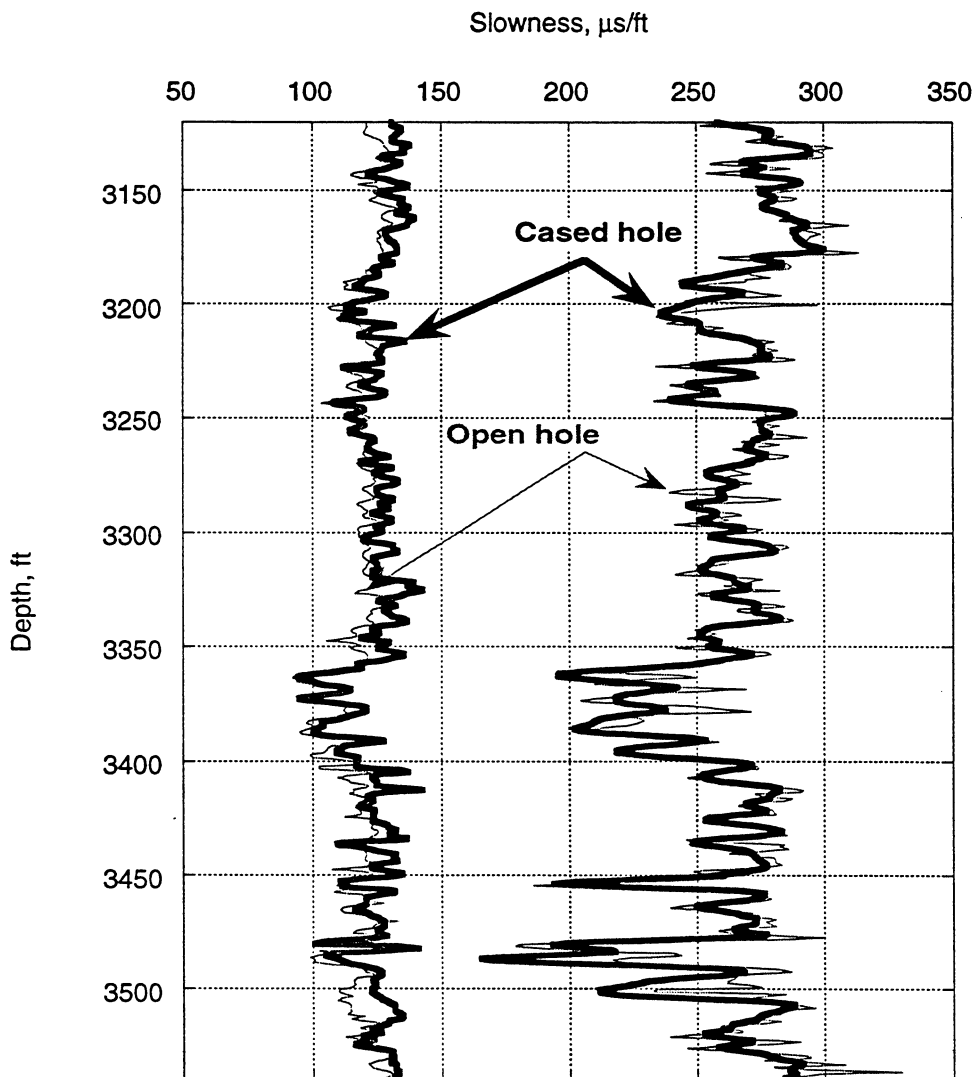


Figure 2. Cased-hole (heavy black lines) and open-hole (thinner gray lines) P- and S- wave slownesses calculated from monopole and dipole waveforms recorded in the Upper Terminal of M-499. Although dt_s is similar, dt_p measured in the open hole is slightly lower than that determined from the cased hole data.

Figure 2 shows P- and S- wave slownesses for the Upper Terminal Zone of M-499. Both cased- and open- hole slownesses are shown. As was discussed previously, dt_s is similar,

whereas dt_p is generally lower in the open-hole than in the cased-hole. The analysis presented in the remainder of this paper uses the cased-hole results.

Monopole and dipole sonic data were recorded in 167-W using both the MPI XACT tool and the Schlumberger DSI tool. Initial results using both tools allowed determination of the P-wave slowness throughout the well, and of the shear-wave slowness in the section of fiberglass liner below 4080 feet. Results in the cased hole were ambiguous.

A second log of the hole was run with the XACT tool, configured to allow independent surface recording of arrivals from opposite sides of the tool. In theory, this should allow unambiguous identification of the type of arrival, as monopole energy should arrive in phase on opposite sides of the tool, and dipole energy should arrive out of phase. Standard tools using crystals as receivers take advantage of this effect, by summing or differencing signals from opposite sides of the hole before transmitting data to the surface. This has the advantage of increasing signal-to-noise, thereby maximizing dynamic range, at the expense of uncertainty in the identity of a "mixed" mode which is not completely eliminated by the downhole mathematics (either because of receiver mismatch, tool eccentricity or other effects).

Analysis of the data recorded using separate crystals allowed determination of the intervals over which the tube wave interfered with the dipole mode. The tube wave overlapped the dipole mode in frequency. Above about 2900 feet, the dipole mode propagated more slowly than the tube wave. Below about 3300 feet, the dipole mode propagated more quickly than the tube wave. In the intervening interval, the dipole and tube wave arrivals overlapped in both frequency and time. Filtering to isolate the dipole mode, and travel-time analysis restricted only to the time interval within which tube wave interference was minimal, allowed determination of dipole mode slowness over much of the well.

Figure 3 compares delta-t values determined from monopole and dipole logs in the interval 4000 to 4600 feet in 167-W. Also shown is a gamma log, which reveals waterflooded intervals adjacent to perforated sections of the fiberglass liner due to their elevated gamma readings. The correlation between the two compressional logs is excellent, and even the shear-wave logs are similar. This includes the interval behind steel casing above 4080 feet. The thicker lines show the results from analysis of the data recorded independently on opposite sides of the tool; it shows a somewhat better correlation between dt_p and dt_s and will be used in the remainder of the paper to determine saturation.

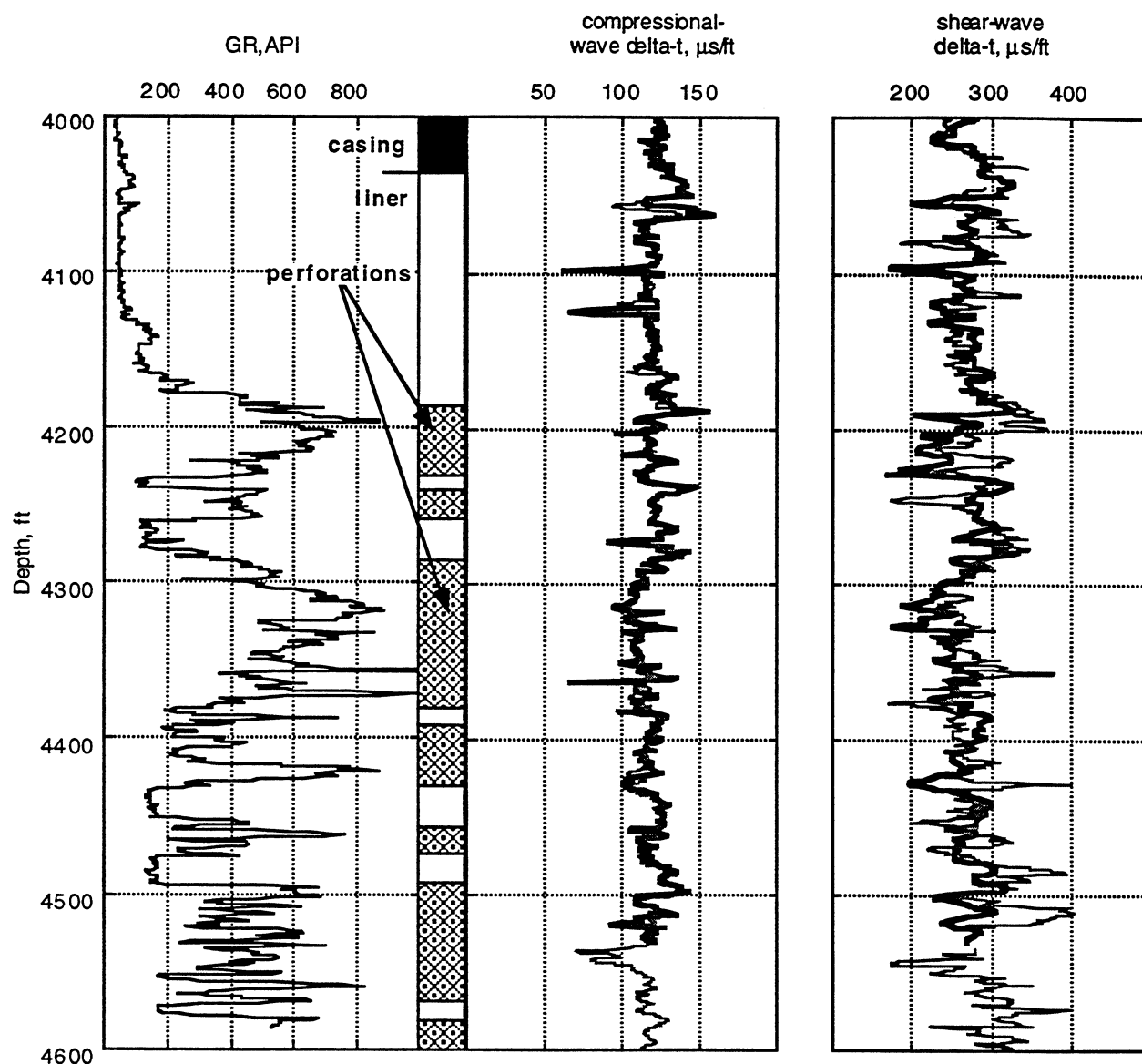


Figure 3. Compressional and shear-wave delta-t calculated from monopole and dipole waveforms recorded in the lowermost section of 167-W for two different logging sondes. Also shown is gamma (GR) and the locations of perforated intervals in this injection well. High gamma associated with perforated intervals indicates zones into which water has been injected.

SATURATION ESTIMATION IN WATER-FLOODED VS. PRODUCTIVE ZONES

Injection has been ongoing into the lowermost section of 167-W for more than 10 years. Thus it is reasonable to assume that all of the mobile oil has been flushed from the near-wellbore region. Since elevated gamma is found adjacent only to perforated zones, it is reasonable to assume that the injection process is associated with the high gamma readings. Thus a discriminator based on the gamma-ray log can be used to select only the sonic data recorded within the flushed zones.

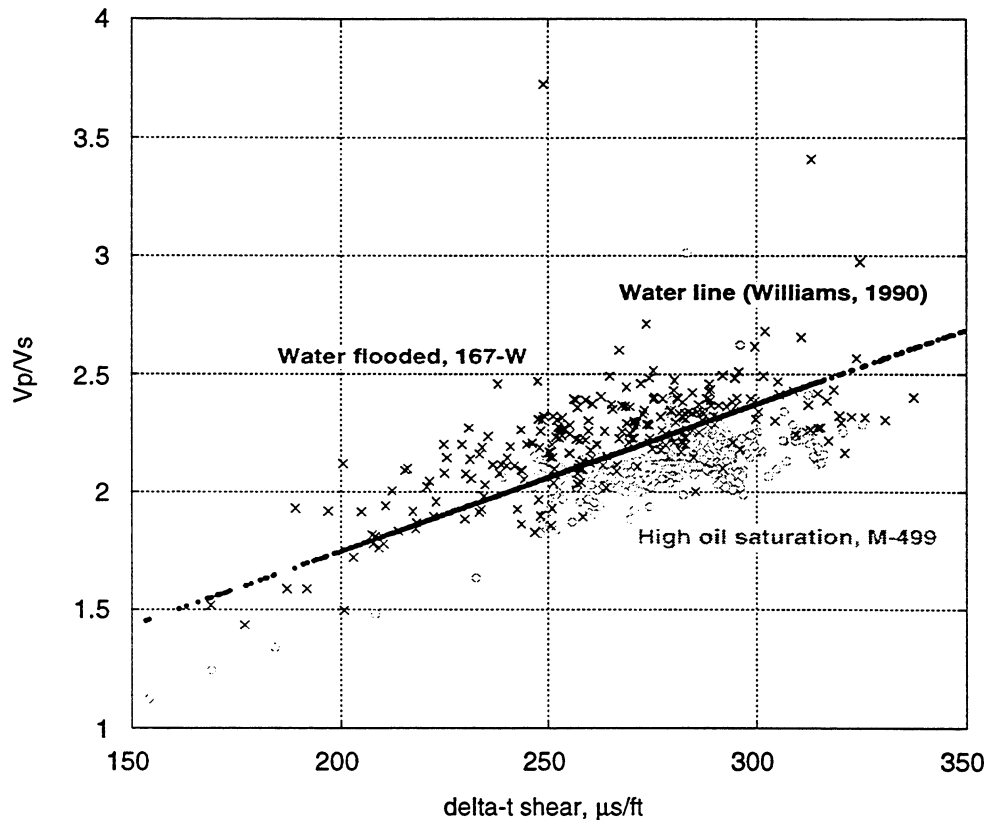


Figure 4. ALHI plot (V_p/V_s vs. Δt_s) of data from intervals with high oil saturation in M-499 (circles) and intervals with high water saturation in 167-W (crosses). Also shown is the empirical water line of Williams (1990), which is predicted to separate the two sets of data.

By comparing these data to sonic data recorded in zones within M-499 with high oil saturations detected using electrical methods, we can determine whether producible hydrocarbons could be detected using only the sonic data.

Figure 4 shows V_p/V_s plotted against Δt_s (an ALHI plot) for data from water-flushed sands and wackes in 167-W (crosses) and high oil saturation zones within M-499 (open circles). Also shown is Williams' (1990) ALHI water line determined empirically, which should separate the two data sets. With only a few exceptions, all of the points from within high oil-saturated intervals of M-499 plot below the ALHI line, and all of the data from water-saturated intervals of 167-W plot above the line. This is particularly impressive when one considers that the oil saturation in M-499 is everywhere less than 0.5.

This initial result is quite promising. However, earlier work revealed that the sonic technique tended to yield “false positives” - i.e. it predicted that zones would be productive which were determined based on other data (but interestingly, not by actual testing!) not to be. And, it was not clear whether the effects could be predicted theoretically or from laboratory measurements, thereby putting the technique on a sound physical footing and allowing application in regions for which it had not been calibrated. These issues are under investigation in the remaining year of the project.

CONCLUSIONS

Results to date indicate that it is possible to discriminate between potentially productive intervals and those which are watered out using measurements of compressional and shear wave velocities recorded through casing using sonic monopole and dipole tools. In this field, the ALHI water line of Williams (1990) neatly separates zones which are likely to be productive from those which are not. A number of issues still need to be worked out. Of these, the single greatest problem continues to be how to acquire the data necessary to carry out the analysis.

REFERENCES

- Batzle, M., and Wang, Z., 1992, Seismic properties of pore fluids: *Geophysics*, **57**, 1396-1408.
- Biot, M.A., 1956, Theory of elastic waves in a fluid-saturated porous solid, II. Higher frequency range: *J. Acoust. Soc. Am.*, **28**, 179-191.
- Gassmann, F., 1951, Über die elastizität poroser medien: *Vierteljahrsschr. Naturforsch. Ges. Zuerich*, **96**, 1-23.
- Mayuga, M.N., 1968, Geology and Development of California's Giant - The Wilmington Oil Field *in* AAPG 53rd Ann. Meeting, Oklahoma City, OK, p. 47.
- Moos, D., 1995, Using multipole acoustic logs in cased holes to determine porosity and oil saturation in clastic reservoirs, Paper F4 *in* Nur, A., Zoback, M.D., and Mavko, G., eds., *Proc. SRB Annual Meeting*, June 1995, Stanford, CA.
- Moos, D., Hara, S., Phillips, C., Hooks, A., and Tagbor, K., 1995, Field test of acoustic logs for measuring porosity and oil saturation in a mature waterflood in the Wilmington Field, CA, SPE 29655 *in* SPE Western Regional Meeting, March 1995, Bakersfield, CA.

PAPER H7

IDENTIFYING PATCHY SATURATION FROM WELL LOGS

Jack Dvorkin, Amos Nur, James Packwood

Stanford Rock Physics Laboratory

Dan Moos

Stanford Borehole Geophysics Laboratory

ABSTRACT

We consider two saturation patterns in a partially saturated rock. The first is the homogeneous pattern where saturation is the same at any location in the rock. The second is the patchy pattern where a fully-saturated patch may be surrounded by a dry region. In both cases, the global saturation value in a large volume of the rock is the same. At the same global saturation, the effective acoustic properties of the rock vary depending on the saturation pattern. We provide a practical method for identifying the dominating saturation pattern from well logs. This method performs well in soft rocks whose acoustic properties are most sensitive to the way fluid is distributed in the pore space. Well logs from high-porosity soft sands indicate that patchy saturation patterns do exist.

INTRODUCTION AND PROBLEM FORMULATION

The heterogeneous geological nature of porous rocks and soils often results in the heterogeneity of fluid distribution on scales greater than pore or grain size. In a partially saturated rock two end members of pore fluid arrangement can be considered: (a) the fluid is evenly distributed within the pore space, i.e., fluid distribution is homogeneous; and (b) the fluid is arranged in fully saturated patches that are surrounded by dry or partially saturated regions, so that fluid distribution is patchy. These patches may include thousands of grains.

It is important to identify the type of pore fluid distribution because:

- a. The nature of oil/gas distribution in a pay zone affects the estimates of reserves, relative permeability, and dry-frame elastic properties. The dry-frame elastic properties are

- needed for the "fluid substitution" procedure where the velocities in a rock with a new, hypothetical, fluid are calculated from those measured in the rock with the known fluid.
- b. The patchy arrangement of ground water is probably common in undersaturated aquifer zones. To determine the details of such patchy arrangements is important for ground water flow calculations and watertable monitoring.
 - c. Industrial groundwater contaminants in the shallow subsurface may occur in patches, or may be evenly dispersed in the pore space. Determining the arrangement type will help select the remediation technique.

The problem posed is to identify the saturation pattern from well logs. In order to solve this problem, we assume that at every depth point of interest the following are available: P -wave velocity (V_p), S -wave velocity (V_s), density (ρ), porosity (ϕ), and saturation (S). In addition, we have to know the bulk modulus of the solid phase of the rock (K_s), as well as the bulk moduli of the liquid and gas phases (K_l and K_g , respectively).

SATURATION PATTERN, VELOCITY AND POISSON'S RATIO

Homogeneous Saturation

Consider a rock at saturation S . If the saturation pattern is homogeneous, the volumetric fraction of liquid in every pore is S , and the rest of the volume in the pore is occupied by gas. The effective bulk modulus K_f of such a liquid-gas mixture can be found from

$$\frac{1}{K_f} = \frac{S}{K_l} + \frac{1-S}{K_g}. \quad (1)$$

The effective bulk modulus of the partially saturated rock (K_{Sat}) is related to that of the dry frame (K_{Dry}) by Gassmann's (1951) equation:

$$\frac{K_{Sat}}{K_s - K_{Sat}} = \frac{K_{Dry}}{K_s - K_{Dry}} + \frac{K_f}{\phi(K_s - K_f)}. \quad (2)$$

The shear modulus (G) of the saturated rock is the same as that of the dry frame. These moduli can be found from the measured velocities and density as

$$K_{Sat} = \rho(V_p^2 - \frac{4}{3}V_s^2), \quad G = \rho V_s^2. \quad (3)$$

Once K_{Sat} is known from well-log measurements, we can calculate the dry-frame bulk modulus from equation (2) as

$$K_{Dry} = K_s \frac{1 - (1 - \phi)K_{Sat} / K_s - \phi K_{Sat} / K_f}{1 + \phi - \phi K_s / K_f - K_{Sat} / K_s}. \quad (4)$$

Then the dry-frame Poisson's ratio (ν_{Dry}) is

$$\nu_{Dry} = \frac{3K_{Dry} - 2G}{2(3K_{Dry} + G)}. \quad (5)$$

Patchy Saturation

If the saturation pattern is patchy, the bulk modulus of the fully-saturated patches (K_0) is that of the fully-saturated rock:

$$K_0 = K_s \frac{\phi K_{Dry} - (1 + \phi)K_l K_{Dry} / K_s + K_l}{(1 - \phi)K_l + \phi K_s - K_l K_{Dry} / K_s}. \quad (6)$$

The bulk modulus of the dry patches (K_1) is that of the gas-saturated rock

$$K_1 = K_s \frac{\phi K_{Dry} - (1 + \phi)K_g K_{Dry} / K_s + K_g}{(1 - \phi)K_g + \phi K_s - K_g K_{Dry} / K_s}. \quad (7)$$

The shear modulus is not affected by the pore fluid. Therefore, the effective shear modulus of the mixture of dry and fully-saturated patches is that of the dry frame. The effective bulk modulus in this (uniform shear modulus) case is independent of the shape of the patches and can be found from Hill's (1963) formula:

$$\frac{1}{K_{Sat} + \frac{4}{3}G} = \frac{S}{K_0 + \frac{4}{3}G} + \frac{1 - S}{K_1 + \frac{4}{3}G}. \quad (8)$$

The inversion of equations (6), (7), and (8) for K_{Dry} gives:

$$K_{Dry} = (-B + \sqrt{B^2 - 4AC}) / 2A, \quad (9)$$

where

$$\begin{aligned} A &= cq + M(bq + cf), B = pc + dq - M(aq - bp - df + ce), C = dp - M(ap + de); \\ a &= S[(1 - \phi)K_l + \phi K_s], b = SK_l / K_s, c = \phi K_s - (1 + \phi)K_l - K_l g / K_s, \\ d &= K_l K_s + (1 - \phi)gK_l + \phi g K_s, e = (1 - S)[(1 - \phi)K_g + \phi K_s], f = (1 - S)K_g / K_s, \\ p &= K_g K_s + (1 - \phi)gK_g + \phi g K_s, q = \phi K_s - (1 + \phi)K_g - K_g g / K_s; \\ M &= \rho V_p^2, g = 4\rho V_s^2 / 3. \end{aligned}$$

Example

In Figure 1a we plot V_p in Ottawa sand versus S , depending on the saturation pattern. The bulk and shear moduli of the dry rock at the effective pressure of 10 MPa are 1.75 MPa and 1.72 MPa, respectively (Han, 1986). Porosity is 0.33. The bulk moduli of the solid phase, liquid and gas are 38 GPa, 2.55 GPa, and 0.018 GPa, respectively. They correspond to pure quartz (Carmichael, 1990), brine of salinity 30,000 ppm, and methane at the pore pressure of 10 MPa and temperature of 50°C (Batzle and Wang, 1992).

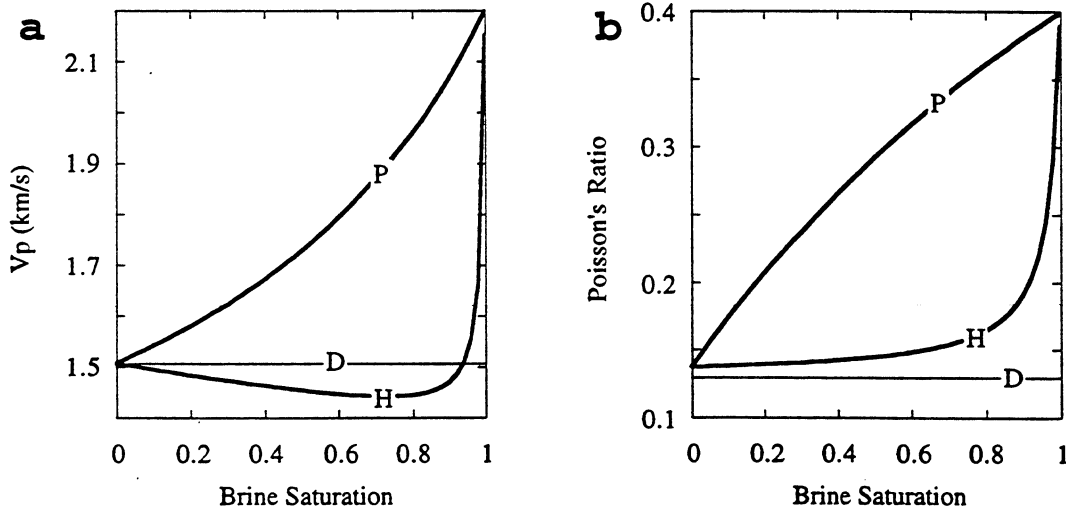


Figure 1: P -wave velocity (a) and Poisson's ratio (b) versus saturation in Ottawa sandstone. Letters on the curves mean: "H" -- homogeneous saturation, "P" -- patchy saturation, and "D" -- dry frame.

If saturation is homogeneous, the compressibility of the brine-gas mixture is very close to that of gas for almost all saturations. Only when water saturation approaches unity does

the compressibility of the mixture sharply decrease and approach that of brine. In this case, the bulk modulus of the rock is approximately constant for almost all saturations and sharply increases as the rock becomes fully saturated. At the same time, the density of the rock steadily increases with increasing saturation resulting in a slight V_p decrease with increasing saturation. Only at a very high saturation V_p approaches its value in the fully saturated rock. The situation is completely different if saturation is patchy. In this case V_p steadily increases with increasing saturation. This drastic difference in the acoustic response of a partially saturated rock emphasizes the importance of determining the saturation pattern in situ. Indeed, if acoustic well logs are interpreted to find the effective elastic properties of the dry rock, the results may be quite different depending on what saturation pattern prevails, and, accordingly, what inversion method is used. It is easy to imagine that the relative permeability of a rock may also strongly depend on the saturation pattern.

SATURATION PATTERNS FROM WELL LOGS

Method

In Figure 1b we plot the Poisson's ratio of Ottawa sand versus saturation. It is clear that this elastic constant is very sensitive to the saturation pattern. Therefore, Poisson's ratio may serve as an indicator of the saturation pattern. We propose the following saturation pattern identification scheme:

1. Find the dry-frame Poisson's ratio from equation (5) by using the inversion for patchy saturation as given by equation (9).
2. If this inversion gives unreasonable values for the Poisson's ratio, then the assumption that saturation is patchy is wrong, and, therefore, saturation is homogeneous.
3. Find the dry-frame Poisson's ratio from equation (5) by using the inversion for homogeneous saturation as given by equation (4).
4. If this inversion gives unreasonable values for the Poisson's ratio, then the assumption that saturation is homogeneous is wrong, and, therefore, saturation is patchy.

Synthetic Well Logs

We test this method on a synthetic well log. The log was created based on laboratory measurements of acoustic velocities and porosity in a suite of soft dry rocks from the Troll Field in the North Sea (Blangy, 1992). The effective pressure is 10 MPa. The liquid and

gas properties are the same as in the above example. We assumed saturation values and saturation patterns versus depth (Figure 2a) and calculated the "measured" V_p and V_s accordingly (Figure 2b).

We calculate the dry-rock Poisson's ratio using the assumption that saturation is patchy in the whole depth interval (Figure 3a). Obviously, the calculated Poisson's ratio values may be quite unrealistic at some depth intervals. In order to identify saturation patterns, we clip the calculated Poisson's ratio log leaving out unreasonable negative values (Figure 3b). What is left most likely corresponds to the patchy saturation pattern since the patchy inversion technique was used here. The rest of the depth interval corresponds to the homogeneous pattern. The intervals of different saturation patterns thus identified exactly correspond to those in the original log, except for one point at the depth of 1656.

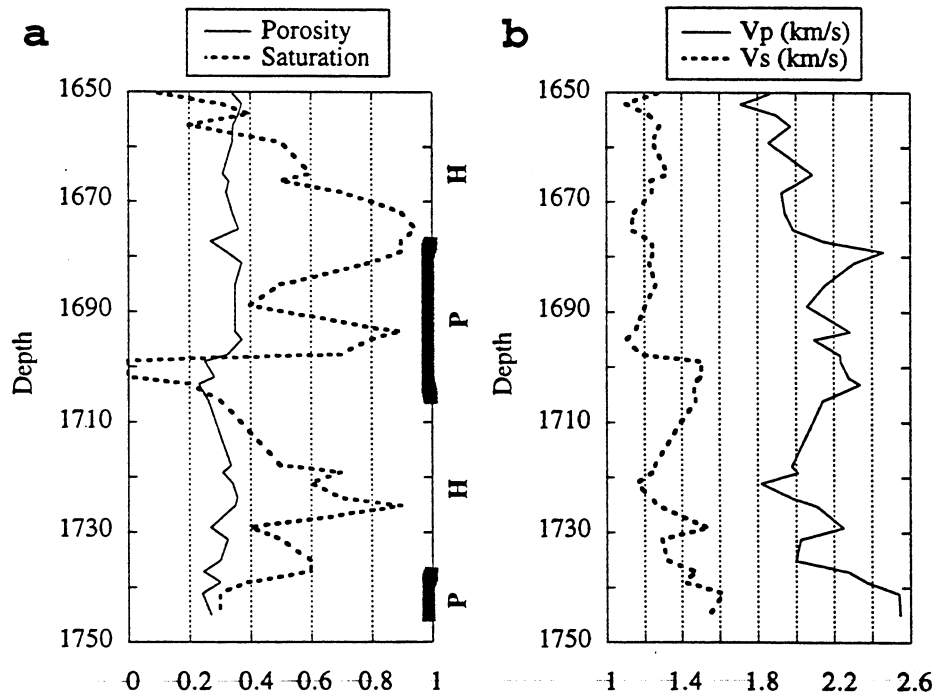


Figure 2: Synthetic well log. Depth given in fictitious units. a. Porosity and saturation versus depth. Bold vertical lines correspond to the depth intervals with patchy (P) saturation. The rest of the interval has homogeneous (H) saturation. b. Velocities calculated from dry-rock velocities and the assumed saturation values and patterns.

Figures 4a and 4b illustrate the importance of identifying the saturation pattern for determining dry-frame properties: unless the saturation pattern is known, the errors in calculating the dry-frame bulk modulus and P -wave velocity may be large. As a result, the fluid substitution procedure may give wrong estimates of seismic velocities and Poisson's

ratios in gas-saturated intervals. To obtain correct Poisson's ratio values is extremely important for AVO analyses.

The proposed method works well in soft formations because their elastic coefficients are extremely sensitive to the presence of low-compressibility pore fluid. This is not necessarily the case in a faster formation.

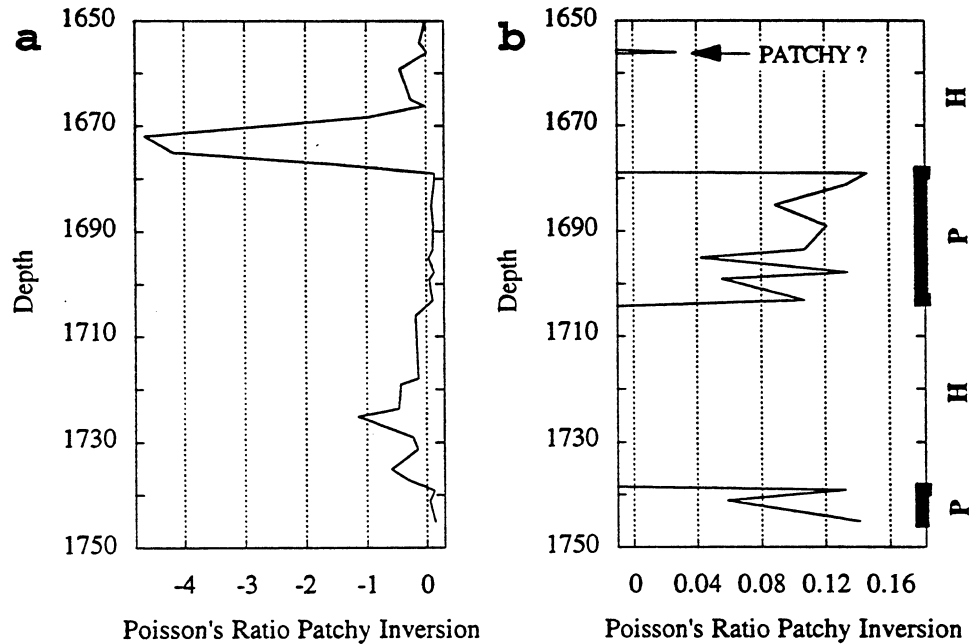


Figure 3: Synthetic well log: patchy inversion for the dry-frame Poisson's ratio. a. The whole range of the Poisson's ratio variation. b. Unreasonable Poisson's ratio values clipped. Bold vertical lines correspond to the depth intervals with patchy saturation. The rest of the interval has homogeneous saturation.

Consider, for example, high-porosity samples from the Oseberg Field in the North Sea (Strandenes, 1991). These granular rocks are quartz- and clay-cemented at their contacts, which results in high acoustic velocities. As in the previous example, we create a synthetic well log based on the laboratory measurement. Again, saturation values and saturation patterns vary with depth. Only at one point the wrong inversion of the dry-frame Poisson's ratio gives an unreasonably negative value (Figure 5a). Otherwise, it is impossible to determine the saturation pattern from the Poisson's ratio inversion. Still, the calculated dry-rock bulk modulus strongly depends on what saturation pattern is assumed during inversion (Figure 5b). However, the errors are not as large as in the soft-formation case.

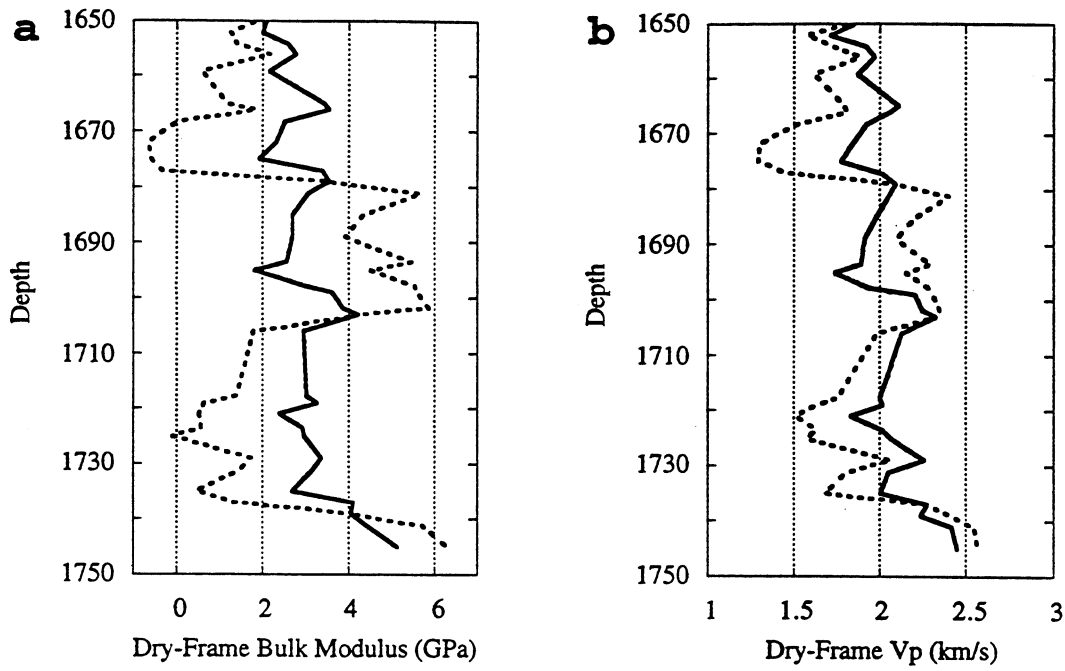


Figure 4: Synthetic well log. a. Determining dry-frame bulk modulus. b. Determining dry-frame velocity. Dotted lines -- wrong inversion, solid lines -- correct inversion.

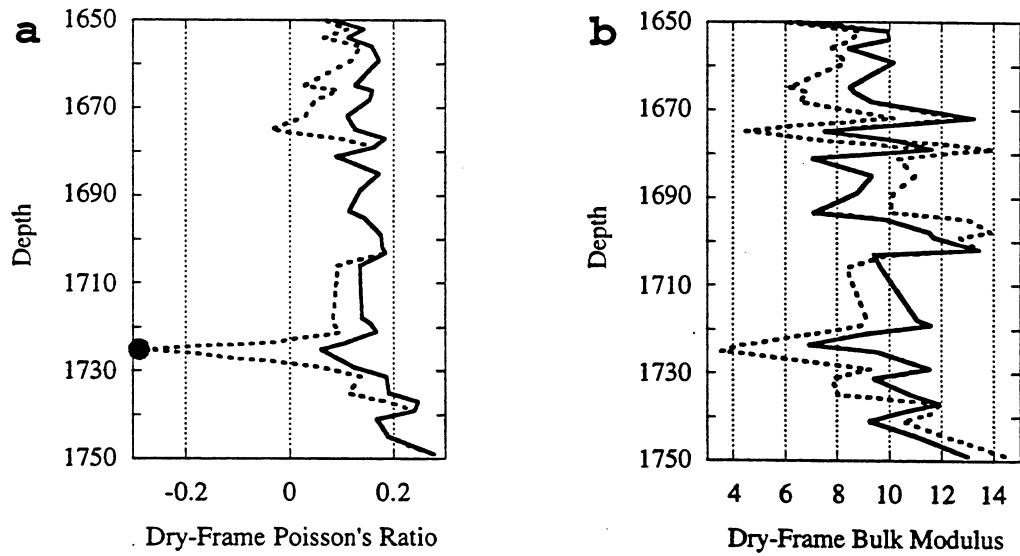


Figure 5: Synthetic well log for fast rocks. a. Dry-frame Poisson's ratio. One unreasonably negative value is shown as the filled symbol. b. Dry-rock bulk modulus. Dotted lines -- wrong inversion, solid lines -- correct inversion.

Real Well Log: Case Study

Two questions remain to be answered. The primary one is: does the patchy saturation pattern exist around real wells? The secondary one is: if it does exist, can it be identified from well logs?

To address these questions, we examine open-hole logs obtained in a well that penetrates unconsolidated gas sands (Figure 6). The frequency of both P- and S-wave sonic tools (Figure 6a) was low, which allowed for the investigation of the uninvaded zone. We select a relatively clean (Figure 6b) high-porosity (Figure 6d) interval with low brine saturation (Figure 6e). The calculated Poisson's ratio (Figure 6f) sometimes exceeds 0.3, which, in a partially-saturated rock, may indicate the patchy saturation pattern (see example in Figure 1b).

To calculate the dry-rock Poisson's ratio, we sequentially use the homogeneous-saturation and the patchy-saturation inversions. The brine and gas bulk moduli (2.88 GPa and 0.0365 GPa, respectively) were selected according to the salinity, and pressure and temperature conditions in the well. The results of the inversions are given in Figure 7a.

In this case it is much harder to separate the patchy-saturation zones from those with homogeneous saturation than in the synthetic log case (Figure 3). A possible indication of patchy saturation are anomalously high dry-rock Poisson's ratios obtained from the homogeneous inversion in the intervals marked with vertical bars in Figure 7a. Indeed, within these intervals, in sands with shale volume below 0.2 (Figure 7b), dry-rock Poisson's ratios exceed 0.2.

Spencer et al. (1994) report that many unconsolidated sands from the Gulf of Mexico have dry-rock Poisson's ratios near 0.18, while other Gulf Coast reservoirs have these values as low as 0.115. Only on several occasions (among a large number of rock samples) do the dry-rock Poisson's ratios exceed 0.2, with the maximum value 0.237. To facilitate this point, we plot dry-rock Poisson's ratios versus porosity (Figure 8) for a suite of unconsolidated North Sea sands (Blangy, 1992) at effective pressure values which bracket the in situ pressure in the well under investigation. Again, these values do not exceed 0.2.

The patchy inversion gives smaller Poisson's ratio values in the marked intervals (Figure 7a). Still, these values may exceed 0.2, but they appear to be more realistic than those given by the homogeneous inversion. We speculate that it is likely that in the patchy saturation domain the dry patches are not completely dry, and the saturated patches are not completely saturated. This is a reason for the absence of clear separation between the two patterns. Of course, our inversion technique can be easily changed to take this impurity

into account. But this will introduce additional non-measurable adjustment parameters which should be avoided in any practical application method.

The dry-rock bulk moduli curves calculated from the two inversion methods are given in Figure 7c. In the proposed patchy-saturation intervals, the difference between the two may reach 25%. Such a difference has to be taken into account, as it may definitely affect seismic reflection interpretation for direct hydrocarbon indication.

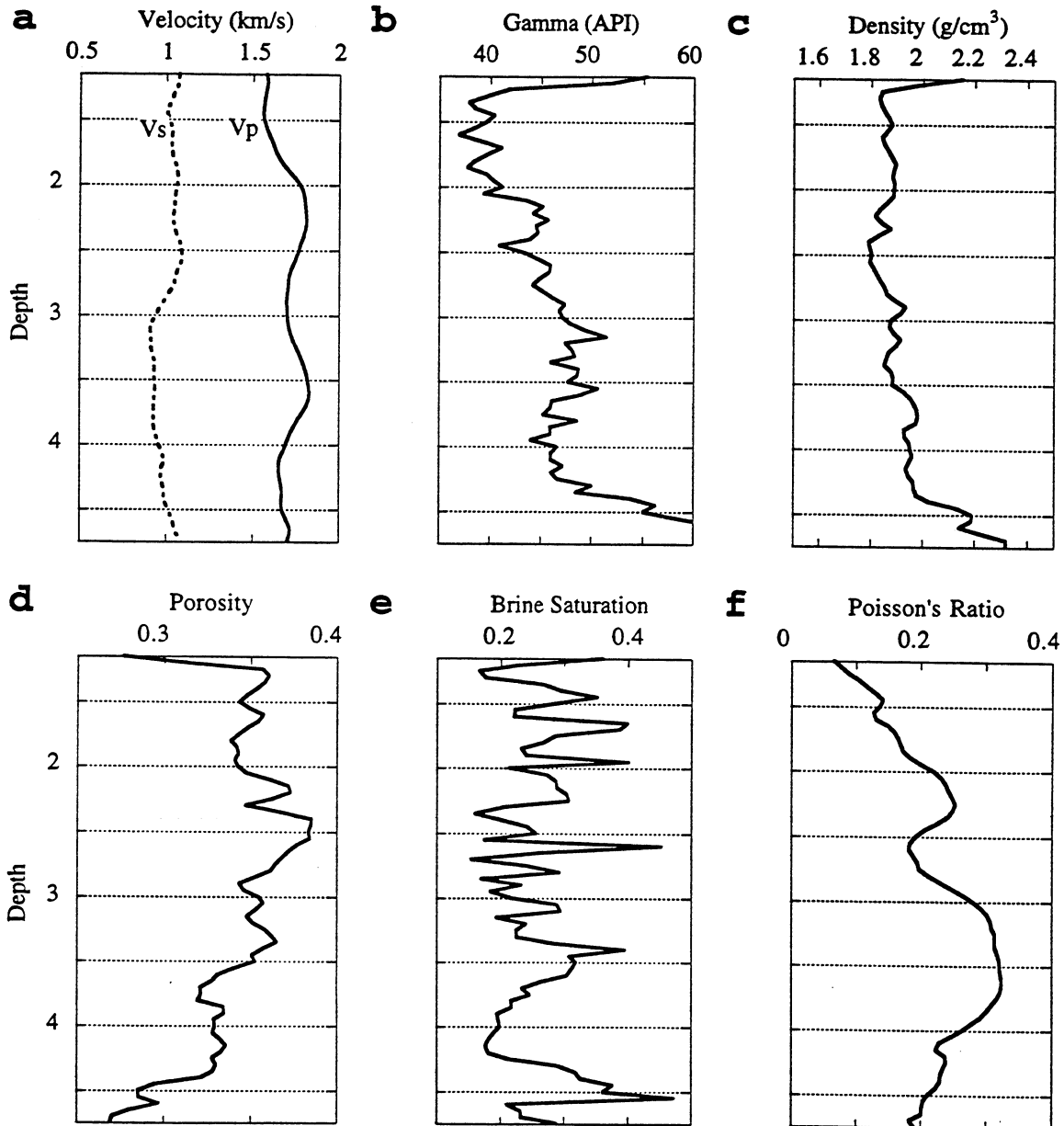


Figure 6: Open-hole logs. Depth is given in fictitious units. a. P- and S-wave velocity; b. gamma-ray log; c. density log; d. porosity (from neutron and density logs); e. saturation (from resistivity); and f. Poisson's ratio calculated from sonic logs.

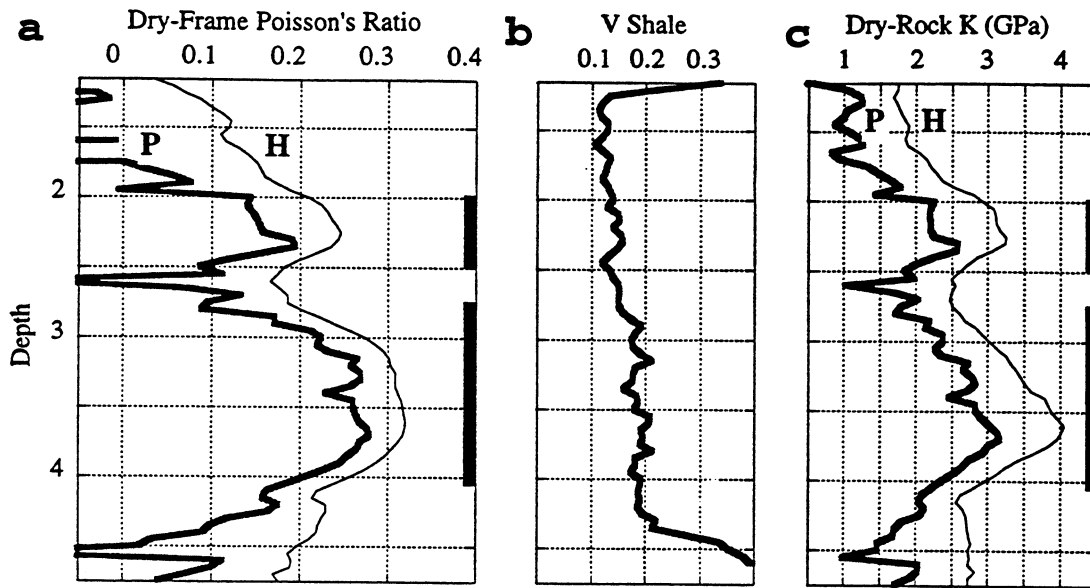


Figure 7: Inversion of the open-hole logs. Depth is given in fictitious units. Bold vertical lines mark depth intervals where patchy saturation is likely. The inversion curves are marked: **H** – homogeneous saturation, **P** – patchy saturation. a. Dry-rock Poisson's ratios; b. clay volume from gamma-ray log; and c. dry-rock bulk moduli.

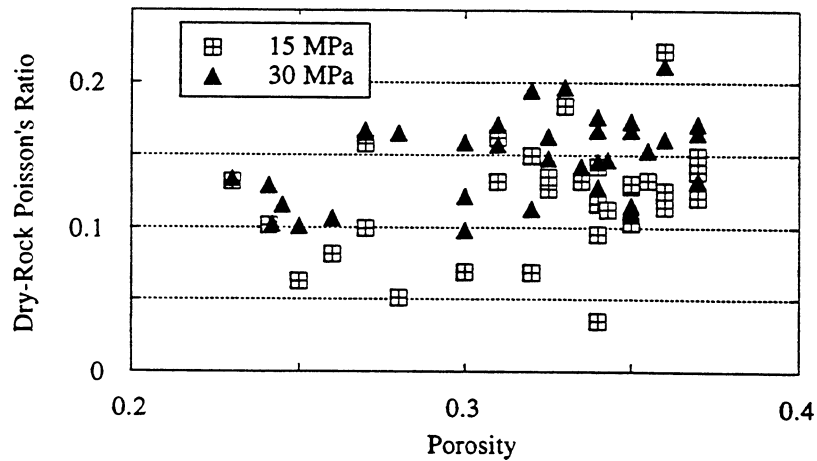


Figure 8: Dry-rock Poisson's ratios versus porosity in unconsolidated North Sea sands at the effective pressure of 15 MPa and 30 MPa (Blangy, 1992).

To summarize this case study we suggest that:

1. In unconsolidated partially-saturated sands two inversions -- the homogeneous saturation and the patchy saturation techniques -- should be applied to calculate the dry-rock elastic moduli from well logs.

2. If the homogeneous inversion gives dry-rock Poisson's ratios which exceed 0.2 - 0.25, and at the same time the patchy inversion gives lower and more reasonable values, the interval is likely to be patchy-saturated;
3. Then the dry-rock bulk moduli (for the fluid-substitution procedure) have to be calculated accordingly.

In any case, we recommend that both inversion techniques be used to bound the possible dry-rock Poisson ratio and bulk modulus values.

CONCLUSION

- At a fixed partial saturation, two saturation patterns may exist in rocks: the homogeneous one where saturation is the same at any location in the rock, and the patchy one where a fully-saturated patch may be surrounded by a dry region.
- It is important to identify the saturation pattern in order to correctly compute the dry-rock elastic moduli from well logs.
- A synthetic example and a case study show that the identification method where the dry-rock Poisson's ratio is computed sequentially based on the assumptions that the pattern is patchy, and that it is homogeneous, works in unconsolidated sands.
- We recommend that this method be routinely used to bound the dry-rock elastic moduli.

ACKNOWLEDGMENT

The idea of quantifying the patchy saturation pattern belongs to Gary Mavko. This work was supported by DOE (Office of Basic Energy Sciences) and by the Stanford Rock Physics and Borehole Geophysics Consortium.

REFERENCES

- Batzle, M., and Wang, Z., 1992, Seismic properties of pore fluids: *Geophysics*, **57**, 1396-1408.
- Blangy, J.P., 1992, Integrated seismic lithologic interpretation: The petrophysical basis: Ph.D. thesis, Stanford University.
- Carmichael, R.S., 1990, Practical handbook of physical properties of rocks and minerals: CRC Press.
- Dewan, J.T., 1983, Essentials of Modern Open-Hole Log Interpretation: PenWell, Tulsa.
- Gassmann, F., 1951, Elasticity of porous media: *Über die elastizität poroser medien: Vierteljahrsschrift der Naturforschenden Gessellschaft*, **96**, 1-23.
- Han, D.-H., 1986, Effects of porosity and clay content on acoustic properties of sandstones and unconsolidated sediments: Ph.D. thesis, Stanford University.
- Hill, R., 1963, Elastic properties of reinforced solids: Some theoretical principles, *J. Mech. Phys. Solids*, **11**, 357-372.
- Spencer, J.W., Cates, M.E., and Thompson, D.D., 1994, Frame moduli of unconsolidated sands and sandstones: *Geophysics*, **59**, 1352-1361.
- Strandenes, S., 1991, Rock physics analysis of the Brent Group Reservoir in the Oseberg Field: Stanford Rock Physics and Borehole Geophysics Project, Stanford University.

